Institute of Physics PAS

May 23, 2023

Brief introduction to metal – hydrogen systems investigated with application of the high hydrogen pressure.

Stanisław M. Filipek

Outline

- 1. Equipment used for high-pressure hydrogen treatment.
- 2. Hydrides of metals synthesized under high hydrogen pressure.
- 2.1. Nickel and its alloys. Palladium and "cold fusion". Other transition metals (Mn, $ZrNi_5$ etc)
- 2.2. Aluminium
- 2.3. Amorphous alloys
- 2.4. Novel hydrides from Laves type intermetallic compounds $ZrFe_2H_4$, $ZrCo_2H_2$, ReT_2H_x (Re-rare earth: T – transition metal); unique YMn_2H_6 and $ReMn_2H_6$
- 3. Short comment about recent discovery of room temperature superconductivity in LuH_nN_y

Hydrogen and Metal-Hydrogen systems under High Pressure

P.W. Bridgman (Nobel Prize 1946) initiated challenging studies of matter under very high pressure. His innovative constructions and ideas resulted in characterization and understanding of the behavior of hundreds of substances in extreme pressure conditions. However, he did not try to compress hydrogen neither metal hydrides.

P.W. Bridgman, *Physics of High Pressure* (Dover Publications Inc.; New Edition, USA, 1971).

In the same period Wigner and Huntington predicted, basing on quantum mechanical calculations, that molecular hydrogen at about 30 GPa would transform into the metallic state. Unfortunately the high pressure facilities capable to check this prediction were not available at that time. Nevertheless theoretical prediction of Wigner and Huntington together with experimental basis founded by Bridgman resulted in growing interest towards studies of hydrogen and hydrides under extended pressure conditions.

E. Wigner, H.B. Huntington, *J. Chem. Phys.,* 3, 764 (1935).

The next important step in this exciting challenge has been done by Baranowski who synthesized nickel hydride from elements what required hydrogen pressure of almost 1 GPa.

B. Baranowski, R. Wiśniewski, *Bull. Acad. Polon. Sci., ser. sci. chem.,* 14, 273 (1966).

Professor Bogdan Baranowski - discoverer of the nickel hydride and pioneer of hydrides syntheses under high hydrogen pressure.

In this talk let us focus mainly on two issues:

1. The use of high hydrogen pressures for the synthesis of new hydrides.

2. Investigation of the properties of hydrides subjected to high hydrostatic pressure.
For these two topics, I will discuss mainly the results of the research done together with my colleagues.

In addition, I will briefly present the results of the most advanced research groups (unfortunately I have no part in it) obtained for an extremely difficult but very exciting and challenging problem which is the attempt to metallize hydrogen and check its possible superconductivity.
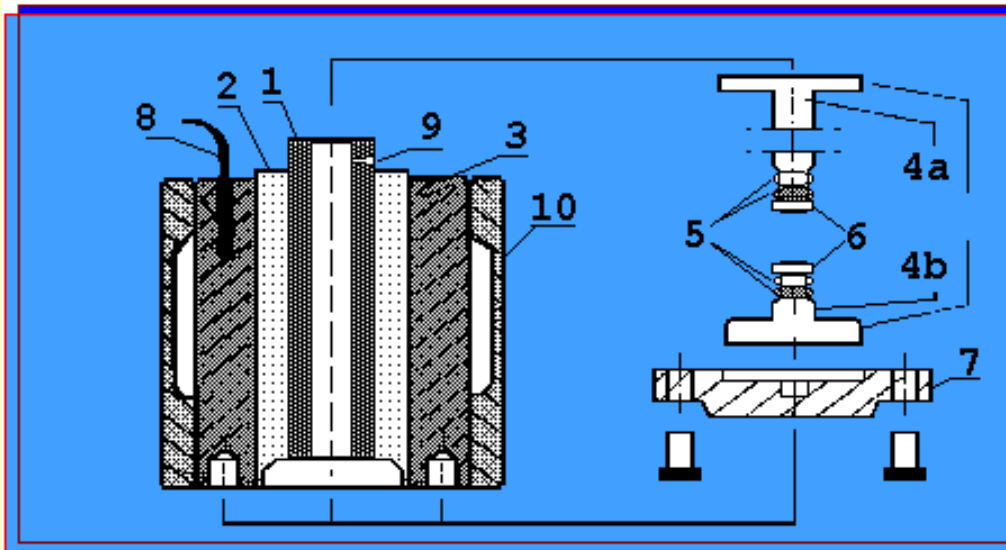
Experimental techniques

➤ High hydrogen pressure equipment:

- piston – cylinder system

- Bridgman anvils, belt type device, cubic press

- DAC (EOS and phase transitions)

➤ XRD and NPD

➤ Synchrotron (XRD and XANES)

➤ DSC

Piston-cylinder apparatus for high hydrogen pressure experiments

$$P(H_2) \leq 1.5 \text{ GPa}$$

$$T \leq 150^{\circ}C$$

(1) – internal tube (berylium bronze); (2) and (3) –middle and external cylinders (high strength steel); (4a) and (4b) –tungsten carbide piston and stopper; (5) and (6)- sealing rings; (8) - thermometer; (9) – capilary inlet; (10) - mantyle

High Hydrogen Pressure Generating

(our design)

A: Hydrogen gas cylinder, B: Oil pump and pressure gauge, C: Pressure intensifier (to increase the pressure of hydrogen gas from gas cylinder, the intensifier can increase the pressure up to 1 bar, equals to 1000 atm), D: Oil pump and pressure meter, E: Reactor, can increase the pressure up to 1.5 GPa (15 kbar)
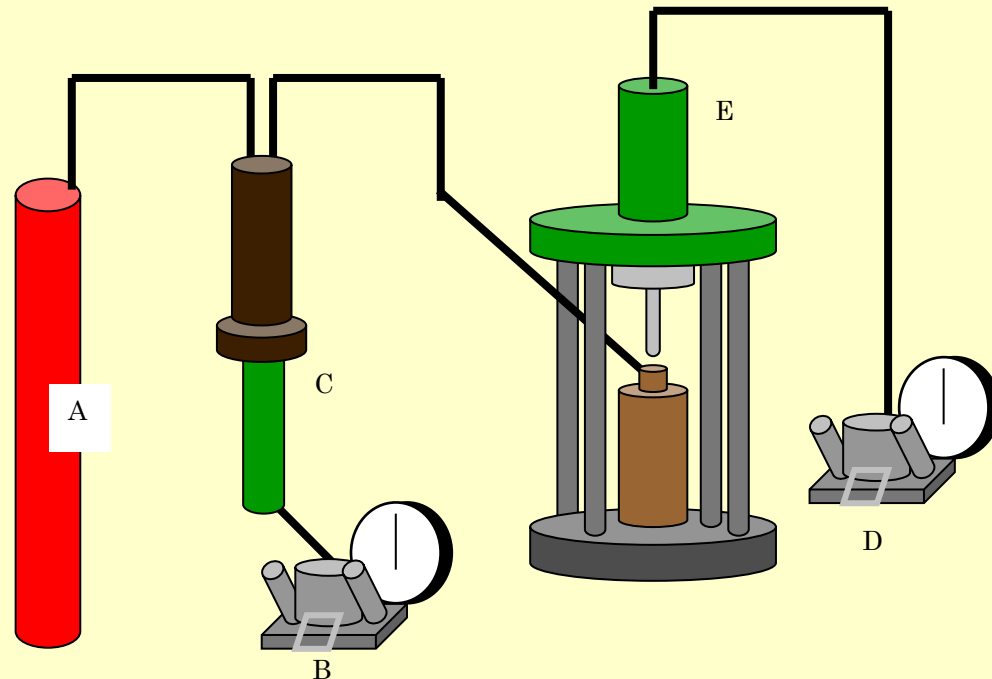
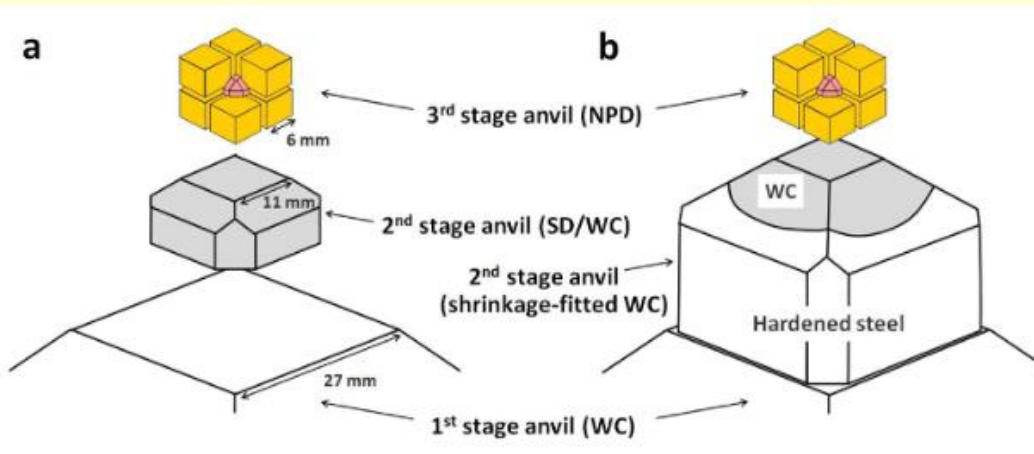# High Hydrogen Pressure Generating System
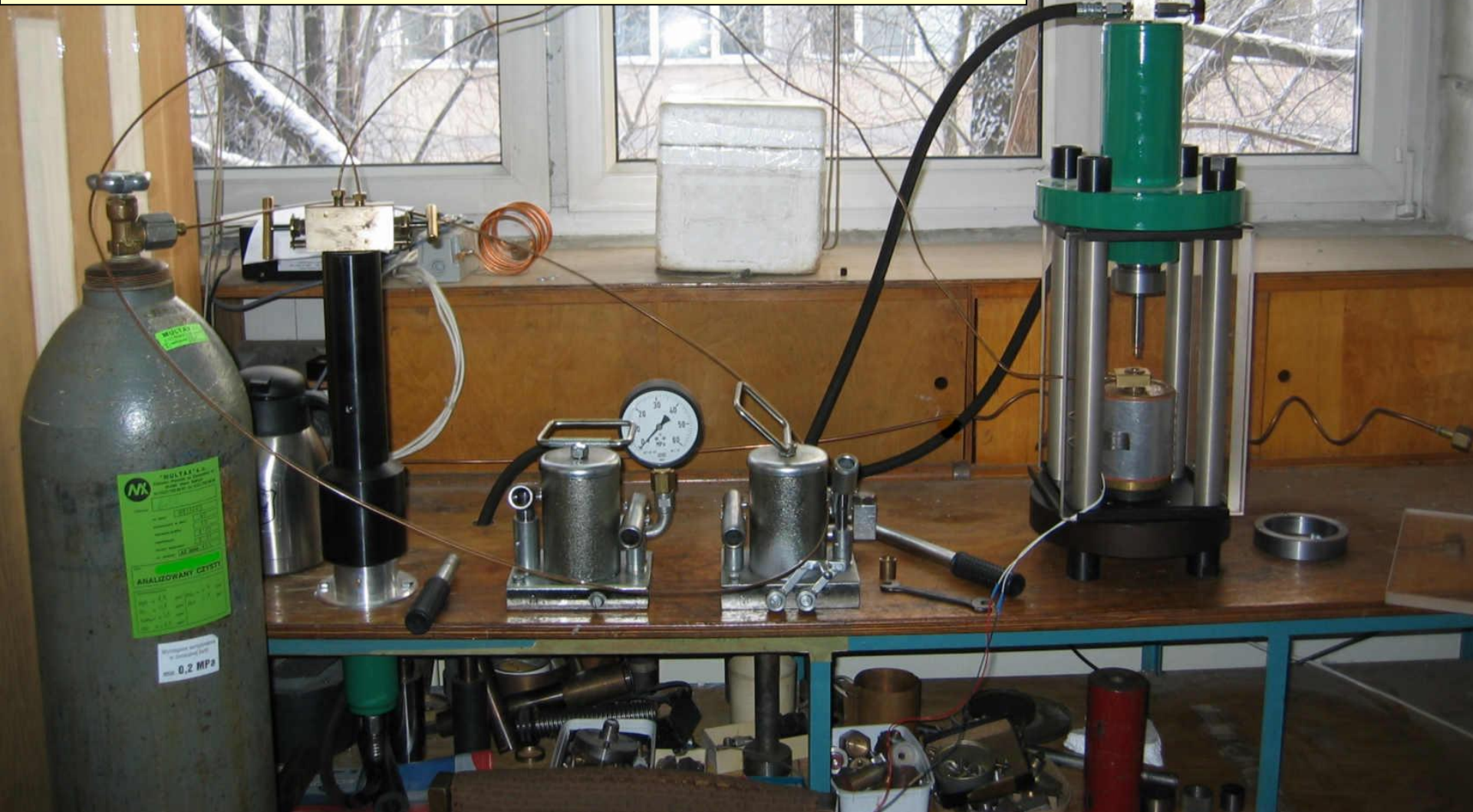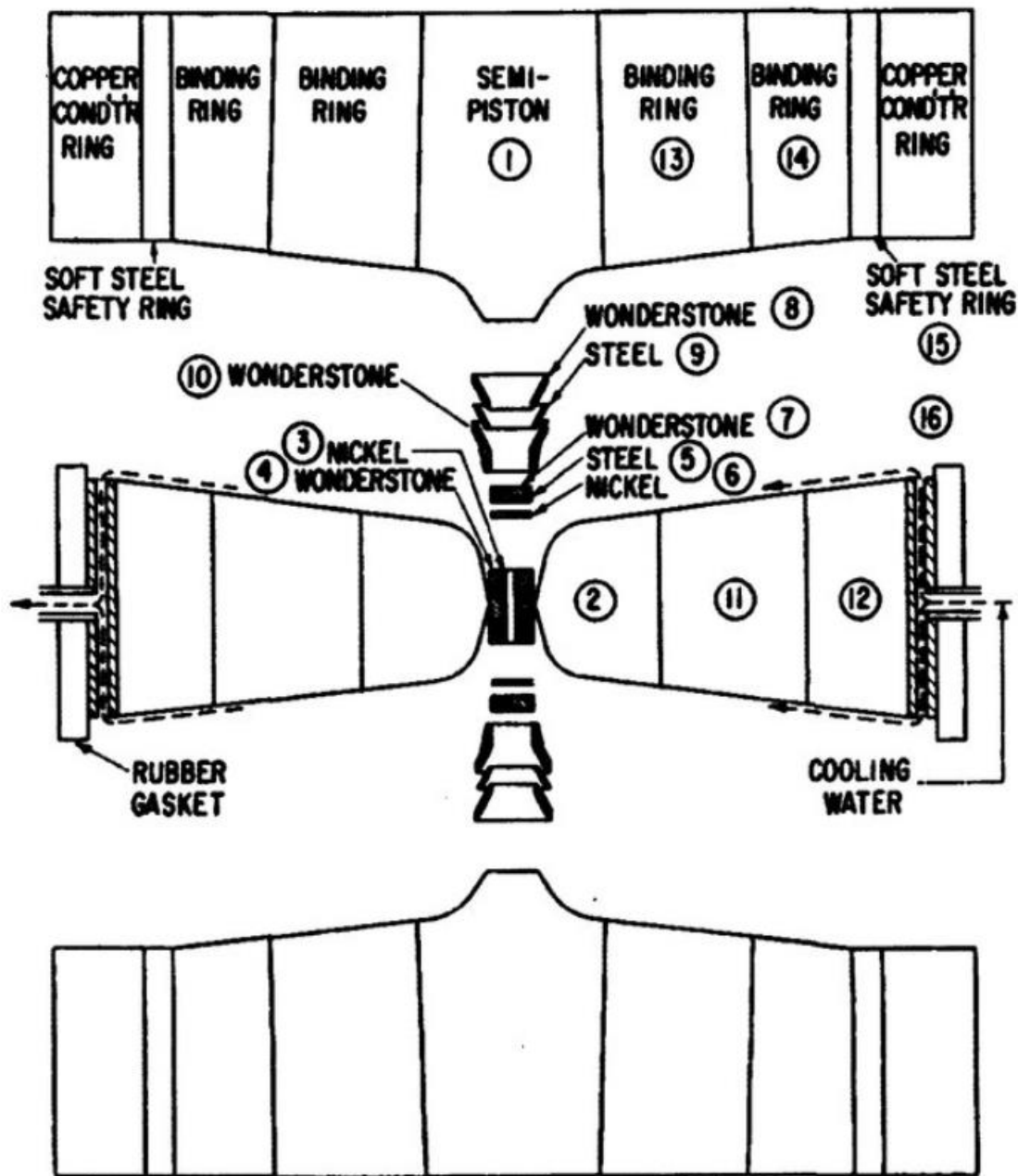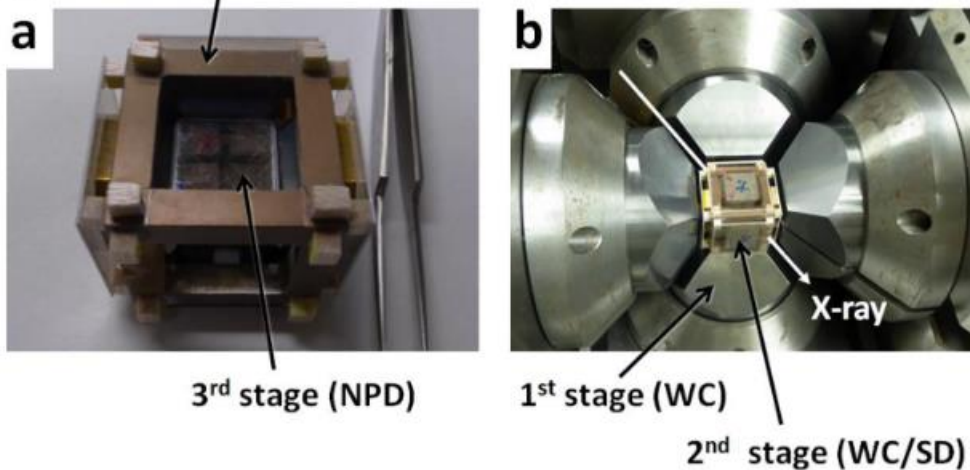
Belt-type high pressure apparatus

H.T. Hall, Ultra-high pressure, high temperature apparatus: The "belt", Rev. Sci. Instrum. 31 (1960) 125-131

T. Irifune *et al.* High pressure generation in Kawai-type multianvil apparatus using nano-polycrystalline diamond anvils, C.R. Geosciences (2019), 351 (2) 260.

Nano-polycrystalline diamond cubes with an edge length of 6 mm have been used as anvils for Kawai-type multianvil apparatus. The maximum pressure of 88 GPa was confirmed based on in situ X-ray diffraction measurements.

Capsules for belt-type or cubic press

E.G. Ponyatovskii, V.E. Antonov and I.T. Belash, in *Problems in Solid State Physics*, edited by A.M. Prokhorov and A.S. Prokhorov (Mir Publ., Moscow, 1984) pp. 109-171.
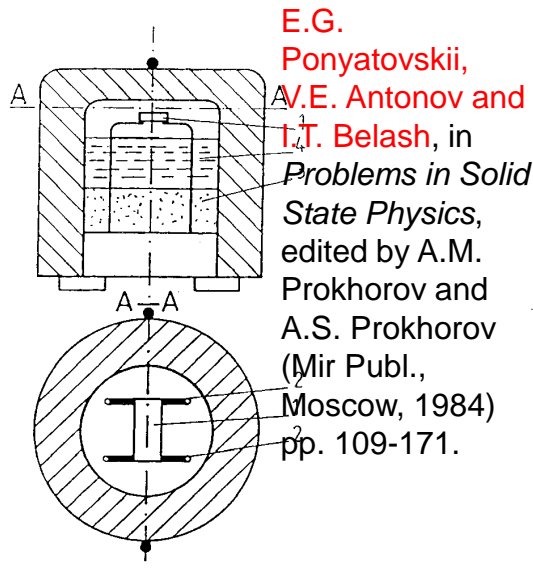
Sawaoka, Filipek

Fig. 5. Ampoule for high hydrogen pressure generation to be used with a conventional quasihydrostatic high pressure apparatus. 1 – sample, 2 – electrical leads, 3 – hydrogen source, 4 – silicon oil (28).

electrical connections 2 for resistance measurements and a substance (like some metal hydrides) playing role of a hydrogen source 3. Samples and the hydrogen source are separated from each other by a silicon oil or an organic liquid 4. After preliminary compression the gaseous hydrogen is evolved from its source (by thermal decomposition for example) and collects in the area of the sample. In this case no external source of hydrogen is needed and the higher available pressure limit is set up by the type of the quasihydrostatic device. The pressure as high as 9 GPa has been reached so far and several new metallic hydrides were obtained using this method. The similar procedure has been also reported by other groups (60–62).

A serious disadvantage of these devices (28,58,59,60–62) is the direct contact between hydrogen and the medium separating the samples from the hydrogen source. This means that the thermodynamic activity of hydrogen may be quite different from that corresponding to pure hydrogen at the given pressure. In other words all these devices (28,58,59,60–62) are not appropriate to
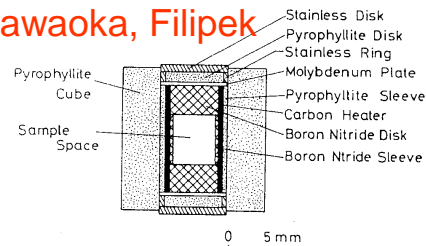

FIG. 2. Cross section of the high-pressure assembly for the cubic anvil apparatus. The synthesizing capsule is placed in the sample space.

out based on the NBS scale of 1971.[5] The atomic ratios (H/M) of synthesized hydride and decomposed hydride were determined by analyzing the gases from thermally decomposed hydrides. The analysis was carried out using the Hitachi 163 gas chromatograph directly connected to a vacuum line. The pressure of carrier gas was maintained at about 1 Torr in the exit port. The gas analyzing system consisted of a vacuum furnace, a Tepler pump, and a reduced pressure gas chromatograph. The error of atomic ratio determination depended on the amount of gas generated in a vacuum furnace. When the gas volume was between 20 and 100 μmol, the standard error of H/M was less than 0.05.

II. RESULTS AND DISCUSSION

Figure 3 shows the relations between the atomic ratios and the temperatures of hydrides obtained at 3.0 and 4.0 GPa. The time duration for synthesis was between 30 min and 2 h. Samarium hydrides were obtained in the atomic ratio from 0.7 to 2.95 under these conditions. $SmH_{2.95}$ (Ref. 6) was synthesized under 3.0 GPa for 1 h at 250 °C and under 4.0 GPa for 1.5 h at 200 °C by using MgH_2 as a solid source of hydrogen. On the other hand, by the use of AlH_3, $SmH_{2.95}$ was obtained under 4.0 GPa for 30 min at 300 °C. Synthe-
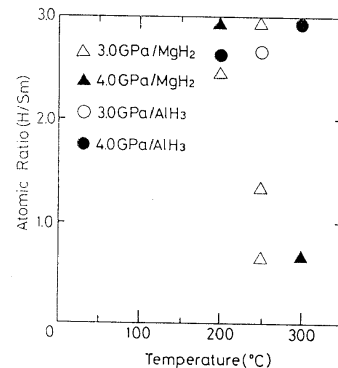
sized hydride pellets with high hydrogen content could be parted easily from the palladium disks. They had a thickness of 0.1–0.3 mm and a diameter of 4 mm. Hydrides having hydrogen content higher than 2.9 had a shiny blue and gray appearance and a high metallic luster.

A phase transformation of MgH_2 with a rutile structure under normal condition into β-MgH_2 with hexagonal structure and γ-MgH_2 with orthorhombic structure under high pressures up to 8.0 GPa at high temperature was reported.[7] Some parts of MgH_2 used for the synthesis of the hydrides were confirmed to transform into β-MgH_2 and γ-MgH_2 under the high pressure up to 4.0 GPa at 2000–300 °C by x-ray analysis. Contrary to the case of MgH_2, AlH_3 was completely decomposed to Al metal under the same condition.

Though MgH_2 is an intermediate hydride, the properties resemble those of a covalent hydride. The heats of formation for MgH_2 and AlH_3 are -11 and -18 kcal/mol at room temperature, respectively.[8] These materials were expected to decompose and to generate high-pressure hydrogen gas in the capsule. AlH_3 was found to be an excellent solid source of hydrogen. However, it is difficult to estimate partial pressure of hydrogen in a capsule. E. G. Ponatovsky et al.[9] used MgH_2, NiH, and others as solid hydrogen sources to investigate the electrical properties of some transition metal–hydrogen systems under high pressures. The capsule method developed by the present authors is simple compared to theirs. By this method, it is possible to prepare a massive rare-earth hydride with a high hydrogen content.

ACKNOWLEDGMENTS

a) Present address: Institute of Physical Chemistry, Polish Academy of Sciences, 01-224 Warszawa, Poland.

[1] G. G. Libowitz and J. C. Pack, "The growth and some properties of cerium hydride single crystals," in *Proceedings of the International Conference on Crystal Growth*, Boston, 1966.
[2] O. Greis, P. Knappe, and H. Müller, J. Solid State Chem. **39**, 49 (1981).
[3] B. Baranowski, Z. Phys. Neue Folge **114**, 59 (1979).
[4] T. Akashi, A. Sawaoka, and S. Saito, Report of the Research Laboratory of Engineering Materials, Tokyo Institute of Technology, No. 3, 1978, p. 69.
[5] E. C. Lloyd (editor), Accurate characterization of the high pressure environment, NBS Special Publication No. 326, 1971, p. 313.
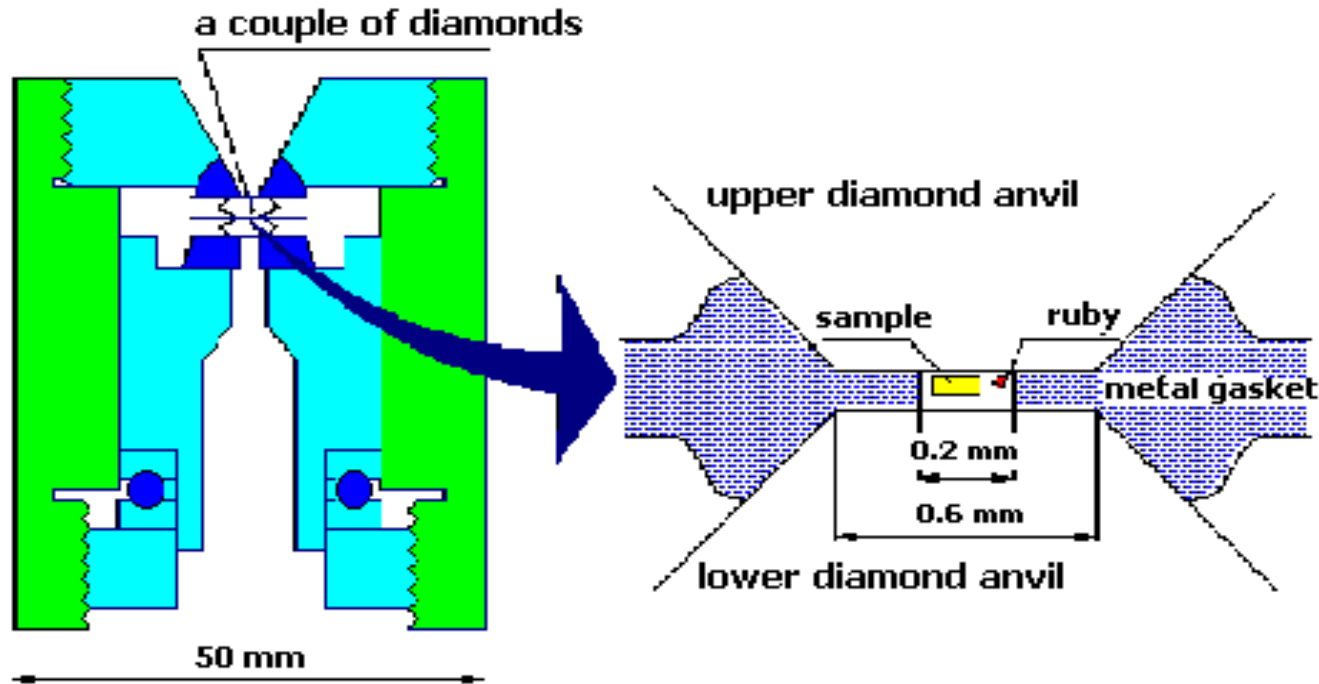[6] $SmH_{0.7}$ and $SmH_{1.31}$ were obtained under 3.0 GPa for 30 min and for 2 h at 250 °C, respectively. In addition, under 4.0 GPa for 1 h at 300 °C, $SmH_{0.7}$ was obtained, too.
[7] J. P. Bastide, B. Bonnetot, J. M. Léteffé, and P. Clandy, Mater. Res. Bull. **15**, 1215 (1980).
[8] W. M. Mueller, J. P. Blackledge, and G. G. Libowitz, *Metal Hydrides* (Academic, New York, 1968), pp. 553–579.
[9] E. G. Ponatovsky, V. E. Antov, and I. T. Belash, "High pressure phases in the metal–hydrogen systems," in *Proceedings of the 8th AIRAPT Conference on High Pressure in Research and Industry*, Uppsala, 1981.

FIG. 3. Relation between atomic ratio and the synthesizing temperatures in obtaining samarium hydrides at 3.0 and 4.0 GPa.

△ 3.0 GPa/MgH_2
▲ 4.0 GPa/MgH_2
○ 3.0 GPa/AlH_3
● 4.0 GPa/AlH_3

DAC aparatus (H. Sugiura, Yokohama, Japan)

Powder samples were pressurized by using DAC apparatus with alcohol medium. Pressure was estimated according the ruby scale. Xray diffraction pattern was measured by energy dispersive type X-ray diffraction system with pure Ge detector. X-ray source was a W tube operated at 47.5kV and 27.5mA. Energy axis of energy spectrum and slit angle in diffraction were calibrated by using fluorescence lines and diffraction lines in cubic InAs patterns.

W.J. Nellis, Metallization of hydrogen
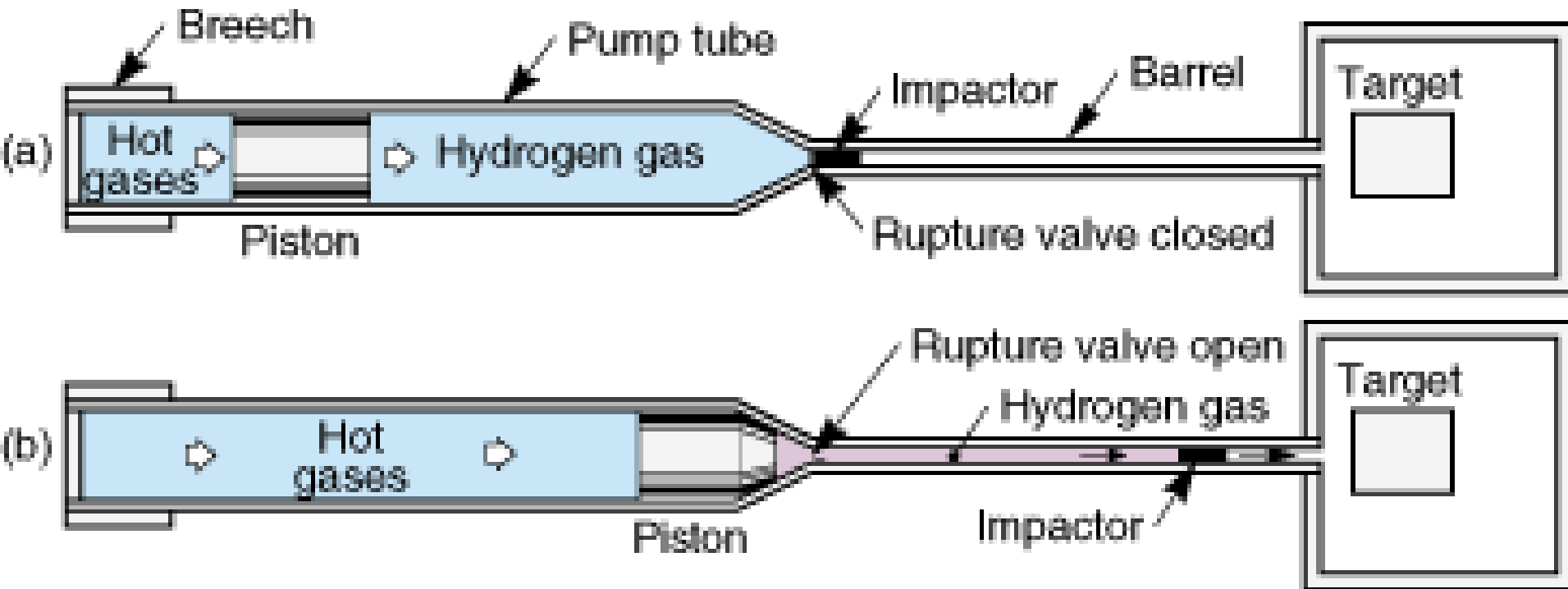
(a) In the first stage of the gas gun (blue shading), hot-burning gases from gunpowder drive a piston, which in turn compresses hydrogen gas. (b) In the second stage (pink shading), the high-pressure gas eventually ruptures a second-stage valve, accelerating the impactor down the barrel toward its target.

W.J. Nellis, Two stage gas-gun
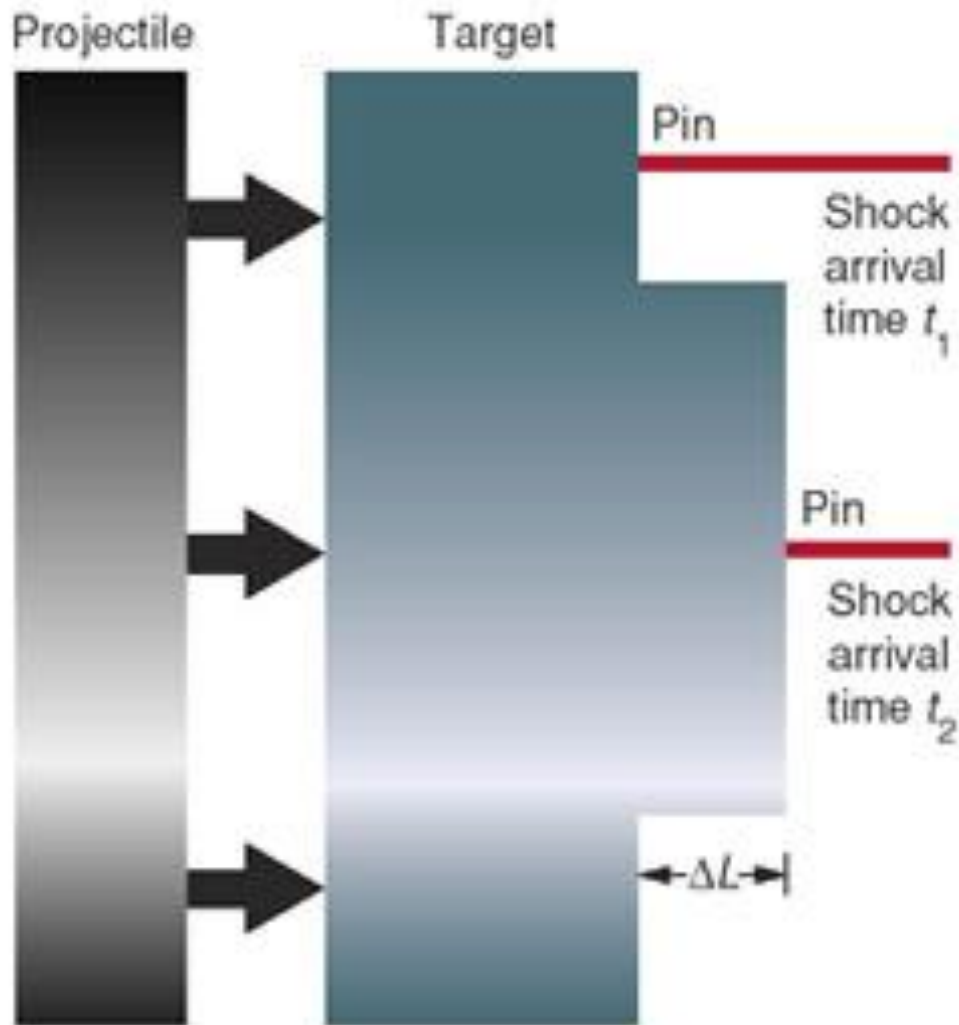
Electrical pins on the target measure the velocity of the shock front as it passes through the target material. Velocity is determined by dividing the difference in pin position by the difference in shock arrival time.

Nellis, W.J., Metallic liquid hydrogen and likely Al2O3 metallic glass, European Physics Journal (2011)

Dynamic compression has been used to synthesize liquid metallic hydrogen at 140 GPa (1.4 million bar) and experimental data and theory predict Al2O3 might be a metallic glass at ~300 GPa. –

Recent papers on metallization of hydrogen

1. M. I. Eremets, I. A. Troyan, A. P. Drozdov, Low temperature phase diagram of hydrogen at pressures up to 380 GPa. A possible metallic phase at 360 GPa and 200 K. arXiv:1601.04479, (2016).
2. Dias, R. P.; Silvera, I. F. (2017). "Observation of the Wigner-Huntington transition to metallic hydrogen". *Science*. **355** (6326): 715–718.
    Metallization of hydrogen at 495 GPa
1. M. I. Eremets, A. P. Drozdov, P. P. Kong, H. Wang, Semimetallic molecular hydrogen at pressure above 350 GPa. Nat. Phys. 15, 1246 (2019).
2. M. I. Eremets, P. P. Kong, A. P. Drozdov, Metallization of hydrogen. (2021).
3. P. Loubeyre, F. Occelli, P. Dumas, Synchrotron infrared spectroscopic evidence of the probable transition to metal hydrogen. Nature 577, 631 (2020).
4. A. P. Drozdov *et al.*, Superconductivity at 250 K in lanthanum hydride under high pressures Nature 569, 528 (2019)
5. Gregoryanz, E. *et al*. Everything you always wanted to know about metallic hydrogen but were afraid to ask. Matter Radiat. Extremes 5, (2020) 038101
6. G. Gao *et al.,* Superconducting Binary Hydrides: Theoretical Predictions and Experimental Progresses, Materials Today Physics, 21 (2021) 100546.
7. L. Monacelli, M. Casula, K.Nakano, F. Mauri, S. Sorella, Quantum phase diagram of high-pressure hydrogen, Nature Physics, March 2023.

Fuji 富士山 3776 m

Ishizuchi 石鎚山 1982 m

Taisetsuzan 大雪山 2290 m

Searching (probably the first) for pressure induced phase transition in metal hydrides

- Purely hydrostatic pressure (where pressure transmitting media is chemically inert) can substantially influence properties of materials. The hydrides are not exception. Very likely the first data related to this topic were presented by us during Japanese National High Pressure Conference in Sapporo in 1976. Further development of diamond anvil cell technique and its application for studies of metal-hydrogen systems revealed phase transformations in alkaline metal hydrides, in manganese hydride, phase separation in palladium hydride and revealed parameters of EOS (Equation of State), also for other hydrides.

第 17 回

高 圧 討 論 会 講 演 要 旨 集

1976年 10月 1 〜 2 日

札　　幌

共　　催

日本化学会・同北海道支部・日本材料学会・同高圧力部門委員会
日本高圧力技術協会・日本鉄鋼協会・化学工学協会・日本機械学会
窯業協会・同東北北海道支部・応用物理学会・日本鉱物学会
日本金属学会・炭素材料学会・電気化学協会・高分子学会
日本学術振興会第117委員会・同136委員会・同138委員会

Influence of high hydrostatic pressure on electrical properties of metal hydrides
S.M. Filipek, A. Sawaoka, K. Wakamori and S. Saito
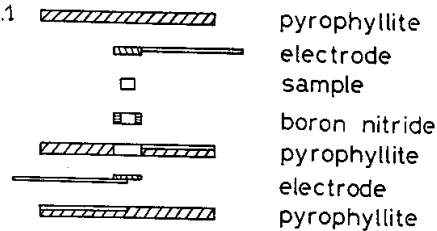## Materials from the High Pressure Symposium, Sapporo, 1976

1B14　水素化物の電気的性質におよぼす圧力効果

東京工業大学　工業材料研究所　　S.M. フィリペク・若森宏志

澤岡　昭・斎藤進六

水素化物の種類は非常に多く、これらの物質の物理的、化学的性質は変化にとんでいる。アルカリ金属、アルカリ土類金属の水素化物と、アルカリ金属、アルカリ土類金属の水素化ホウ素類は化学量論組成をもつ塩基である。希土類金属の水素化物は、非化学量論的な多くの相を作る。この希土類元素水素化物の中で特にセリウム水素化物、ランタン水素化物は興味がある。Staliński[1,2]、Libovitz等[3]の実験結果から、これら二つの物質は構造的変化をともなわない成分依存による金属－半導体転移が見られる。この同じ成分領域（H/He＝2.8）で、250kにおいて、電子的遷移がありこれは成分依存による金属－半導体転移と対応している。このような物質を圧力下で検討することは興味がある。

この研究目的は、次の水素化物 (イ)アルカリ金属三成分水素化物(LiBH₄, NaBH₄, RbBH₄, LiAlH₄) (ロ)アルカリ土類金属水素化物(BaH₂, MgH₂, CaH₂) (ハ)希土類元素水素化物(LaH₃, CeH₃, YbH₃) の高圧力下での電気抵抗の測定により、上記の水素化物の室温高圧力下での特性を調べることである。試料は(LiBH₄を除く)全てアメリカ、Ventron 社の物を使用した。(LiBH₄は和光純薬社製)、純度はCaH₂, LiAlH₄–95%, MgH₂–85%, NaBH₄–98%, RbBH₄–98%, BaH₂–99.5%, LaH₃, CeH₃–99.8% である。水素化物は高い反応性をもつため、操作は全て乾燥アルゴン雰囲気で行なった。水素化物の粉末を金型に入れて圧縮成型後、試料を図1のように組立てた。パイロフェライトアセンブリーは外側をエポキシ樹脂で固めた。実験は主にブリッジマンアンビル装置を使ったが一部はキュービックアンビル装置を使って行なった。結果はアルカリ金属の水素化ホウ素類(LiBH₄, NaBH₄, RbBH₄)の場合、20kbの所で電気抵抗の大きな上昇がみられた。特にLiBH₄の変化は大きい。(図2) この上昇の後、電気抵抗はほとんど変化しなかった。しかし、もっと共有結合性の強いLiAlH₄では上記のような電気抵抗の変化は見られず、全圧力領域でも変化はあまり大きくなかった。アルカリ土類金属水素化物では、MgH₂の性質は他のⅡ族水素化物とは異なり、安定性に欠けている。MgH₂の原子間距離はMg金属の原子間距離よりも大きくなる[4]。高圧下の抵抗測定によっても、MgH₂の特性は他のものとは異なっていた。BaH₂, CaH₂の電気抵抗対圧力の曲線は徐々に減少した。5.7×10⁻³cm³(体)のMgH₂の場合、10kbを越えると、抵抗値はMΩ→Ωへと変化した。加圧後のX線回折の結果によりこのように大きな変化は、試料の部分的な分解によって起こると考えられる。5.7×10⁻³cm³(体)の試料の場合、30kbで同様の変化が起こった。立方体アンビル装置で圧縮された体

図1

(hatched bar)	pyrophyllite
(bar)	electrode
(small square)	sample
(bar)	boron nitride
(bar)	pyrophyllite
(bar)	electrode
(hatched bar)	pyrophyllite

積、0.28cm³の試料は70kbまでは、大きな抵抗の変化はみられなかったが、この場合にも、加圧後のX線回折の結果から金属相の増加がみられた。希土類元素水素化物(LaH₃, CeH₃, YbH₃)は大気圧で、高抵抗半導体である。圧力の上昇にともない、LaH₃, CeH₃の電気抵抗は徐々に下がる。50kb以上では電気抵抗の変化の割合は小さくなる。YbH₃は、(図3)のように20kbの所で、抵抗が最小値をもつ。

今までの結果から、アルカリ金属の水素化ホウ素類の電気抵抗対圧力依存性は、相変化ではないかと思われる。

しかし、LiAlH₄の場合にはこのような可能性はない。又、高圧力下でのMgH₂の不安定性が明らかになった。このため正確な安定領域を決めるために別の手段と、もっと純度の高い試料を使わなければならない。

同じアルカリ土類金属水素化物でも、CaH₂, BaH₂は、MgH₂に比べて高圧力下でも安定であった。CeH₃, LaH₃においては、電気抵抗の変化は大きいが、金属的な特性は示さなかった。

図2

図3
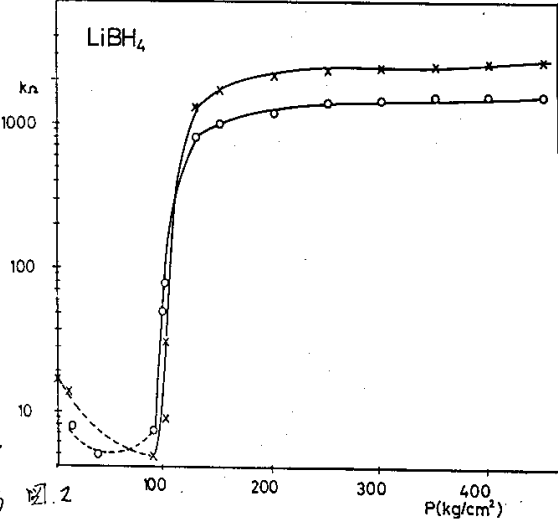
参考文献：

1. B. Staliński : Bull. Acad. polon. Sci. Cl. III. 5, 1002 (1957).
2. B. Staliński : Bull. Acad. polon. Sci. Ser. Sci. Chim. 7, 273 (1959)
3. G.G. Libovitz : Berichte Bunsen-Gesellschaft Phys. Chem. 76, 8, 837 (1972).
4. たとえば G.G. Libovitz : "The Solid-State Chemistry of Binary Metal Hydrides" (W.A. Benjamin, Inc. New York 1965).
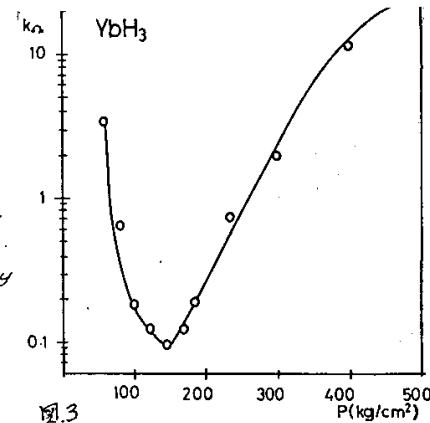
The study on Ytterbium hydride under high pressure is still attractive:

Tomasz Jaroń *et al.* Synthesis, Structure, and Electric Conductivity of Higher Hydrides of Ytterbium at High Pressure, Inorganic Chemistry 2022 61 (23), 8694-8702

# Pressure induced phase transitions in the alkali metal hydrides

Table 1. Bulk moduli K_0, its pressure derivatives $K_0`$, transition pressure P_T and volume changes at the transition of alkali-metal hydrides.

Sample	K_0 GPa		$K_0`$		P_T GPa	Volume change %
	NaCl-type	CsCl-type	NaCl-type	CsCl-type		
[a]CsH	7.6 ± 1.9	22.3 ± 1.5	4.0 ± 0.4	4.8 ± 0.5	1.2	8.4
[a]RbH	10.0 ± 1.0	18.4 ± 1.1	3.9 ± 0.5	3.9 ± 0.5	$2.2 - 3.1$	11.7
[a]KH	15.6 ± 1.5	28.5 ± 1.5	4.0 ± 0.5	4.0 ± 0.6	4.0	13.4
[a]NaH	14.3 ± 1.5	-	7.7 ± 1.0	-	-	-
[b]NaH	19.4 ± 2.9	28.3 ± 3.0	4.4 ± 0.5	4.3 ± 0.4	29.3 ± 0.9	10.0

[a]   H. D. Hochheimer, K. Strossner, W. Honle, B. Baranowski and S.M. Filipek, Z. Phys. Chem. NF, 143, 139 (1985).

[b]   S. J. Duclos, Y. K. Vohra, A. L. Ruoff, S. M. Filipek and B. Baranowski, Phys. Rev., 36, 7664 (1987).

To determine formation pressure of metallic hydrides a very useful is measuring stationary electrical resistance as a function of hydrogen pressure
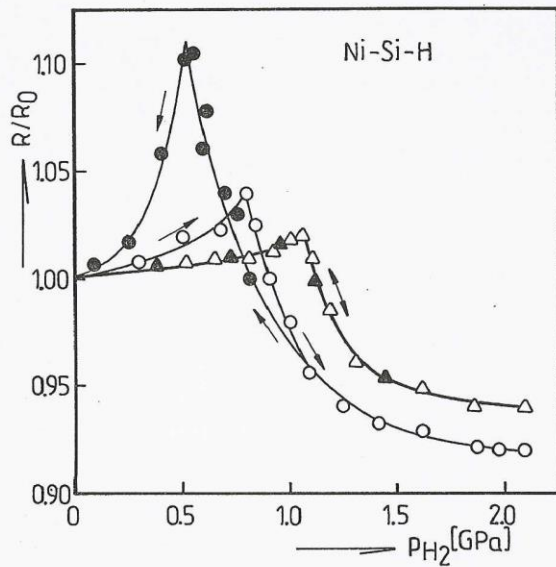

B. Baranowski, S.M.Filipek, *Roczniki Chem.* **45 (1971)** 1353.
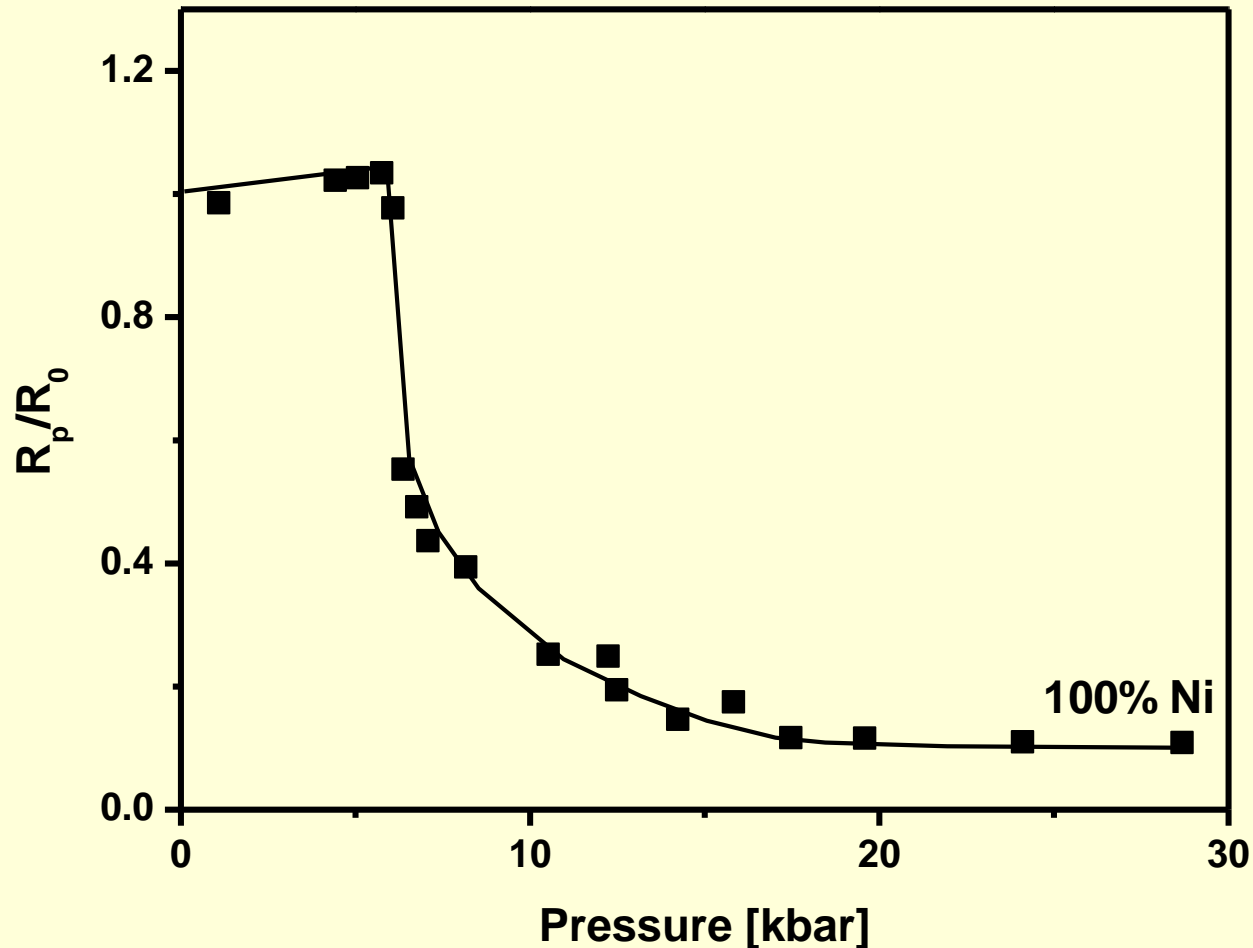
Fig. 9a. Electrical resistance of fcc Ni–Si alloys as function of hydrogen pressure. (o,●) – Ni$_{0.98}$Si$_{0.02}$, (△,▲) – Ni$_{0.90}$Si$_{0.10}$ (open symbols; absorption– , black symbols; desorption branch).
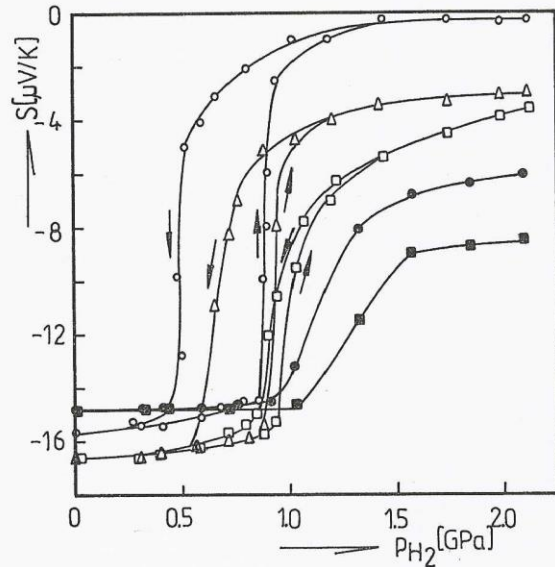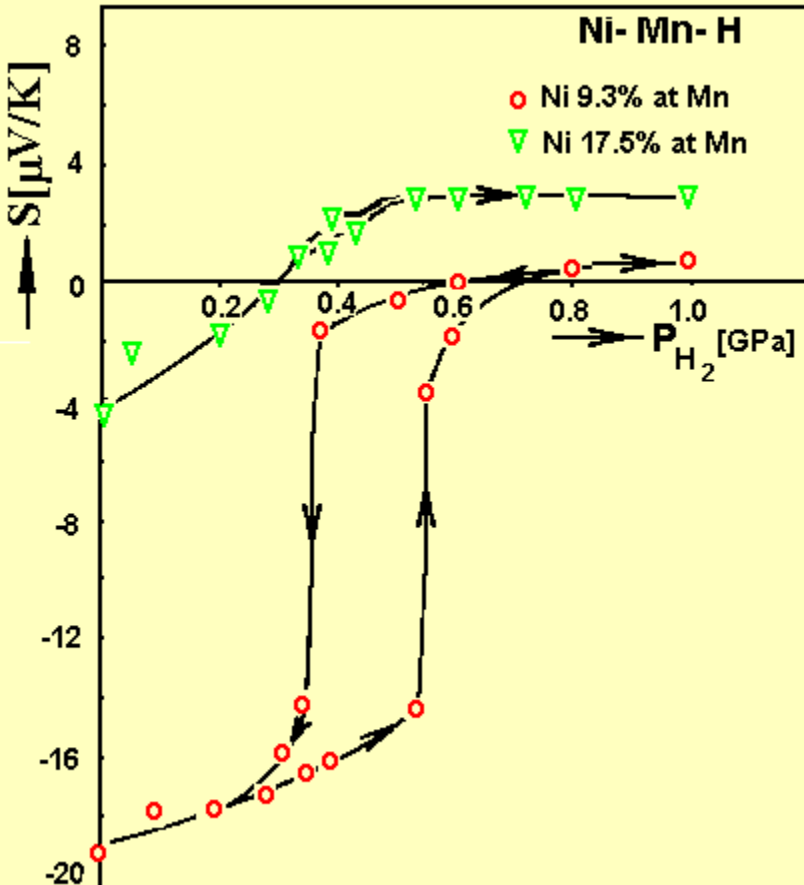

Fig. 9b. Thermoelectric power of fcc Ni–Si alloys as function of hydrogen pressure. (o) Ni$_{0.98}$Si$_{0.02}$, (△) Ni$_{0.96}$Si$_{0.04}$, (□) Ni$_{0.94}$Si$_{0.06}$, (●) Ni$_{0.92}$Si$_{0.08}$, (■) Ni$_{0.90}$Si$_{0.10}$.
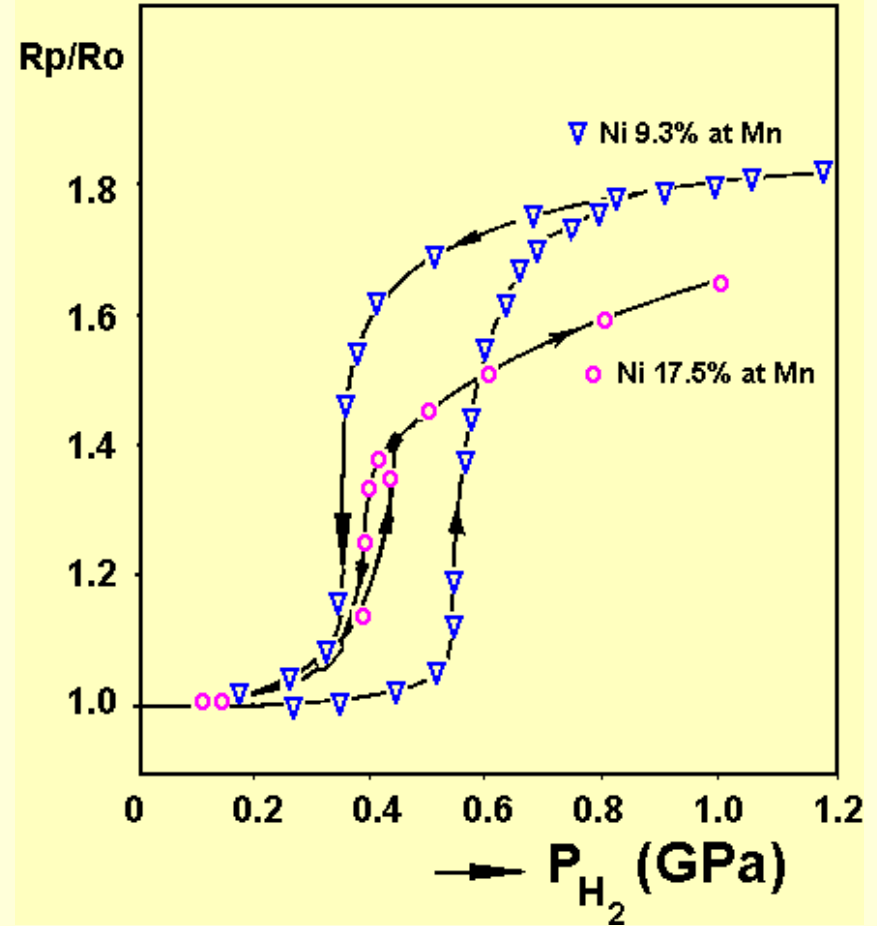
Nickel and nickel alloyed with *p* elements;

Change of resistance and thermoelectric power during hydride formation

S.M. Filipek, A.W. Szafrański, P. Duhaj, *J.Less-Comm. Met,* **101 (1984)** 299.

Ni-Mn-H system

Thermoelectric power of Ni-Mn allos as a function of hydrogen pressure at 298 K.

S.M. Filipek; *Polish J. Chem.* **71**, 1777-1786 (**1997**).

The stationary relative electrical resistance of Ni-Mn allos as a function of hydrogen pressure at 298 K.
R_0 – resistance of sampe at normal pressure of an inert gas. R_p – resistance of sample at pressure p of gaseous hydrogen

the resistance of nickel hydride at 298 K is about 30% smaller than the resistance of nickel.

Introduction of small quantities of chromium or vanadium to nickel results in a dramatic change of thermopower from −19.0 µV/K (for pure nickel) to high positive values (147). This effect was interpreted in terms of virtual bound state of chromium (vanadium) placed near the Fermi level (148). Changes of thermopower of these alloys (Figure 10 and 11) under the hydrogen pressure are quite unusual (25,149). Namely, depending on the concentration of chromium (vanadium) in the alloy, the thermopower change during hydrogenation can be positive or negative. For a certain composition the transformation into the hydride phase occurs practically without any change of the thermopower. This effect was attributed (149) to the shift of the Fermi energy above virtual bound state level of chromium (vanadium) due to electrons introduced with hydrogen which fill the empty states in the d- and s-bands of the nickel matrix.
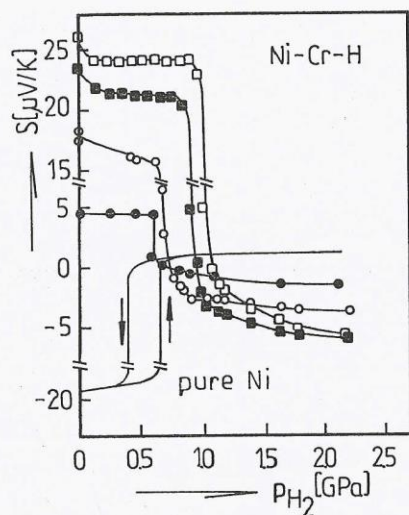
Nickel alloyed with *3d* elements;

Hydrides formation

Fig. 10. Thermoelectric power of fcc Ni–Cr alloys as function of hydrogen pressure (149). (●) $Ni_{0.995}Cr_{0.005}$, (o) $Ni_{0.975}Cr_{0.025}$, (■) $Ni_{0.920}Cr_{0.080}$, (□) $Ni_{0.89}Cr_{0.11}$.

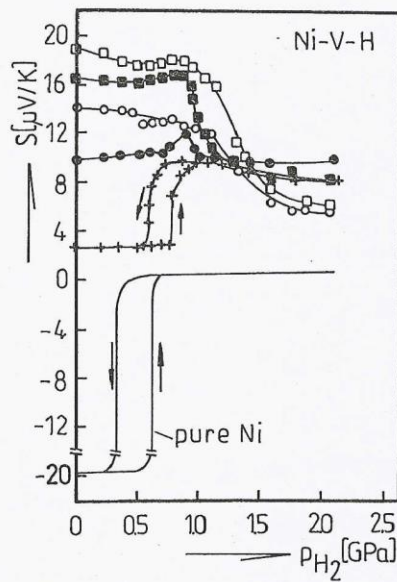Fig. 11. Thermoelectric power of Ni–V alloys as function of hydrogen pressure (149). (+) $Ni_{0.97}V_{0.03}$, (●) $Ni_{0.96}V_{0.06}$, (■) $Ni_{0.91}V_{0.09}$, (□) $Ni_{0.88}V_{0.12}$, (o) $Ni_{0.85}V_{0.15}$.

S.M. Filipek, *Z. Phys. Chemie NF.*, **163 (1989)** 627.

All fcc Ni-Cr alloys considered here form hydride phases in an isomorphic transition in which a discontinuous change of the lattice parameters takes place. Figure 4 shows lattice parameters of the Ni-Cr hydrides formed at 2.7 GPa(H_2) and at 298K. All samples saturated at these conditions were characterized by a very large lattice parameter and a high concentration of hydrogen. For Ni-2.5 at%Cr and Ni-5.0 at%Cr the hydrogen to metal atomic ratio was equal 1.1; for Ni-11 at%Cr it was as high as 1.20. Let us remark that the hydrogenation of Ni-5 at % Cr carried out for six hours at 6.7 GPa(H_2) and at 573K led to the value H/(Ni+Cr)=1.14 /12/ (the lattice parameter was the same as in our case). All the lattice parameters were remarkably larger than those observed after the electrochemical hydrogenation /8/. Lattice parameters of H-free alloys were as in Ref. /13/.

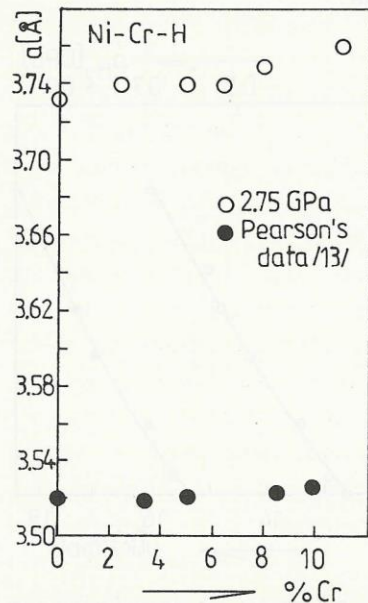The behaviour of the thermoelectric power for the Ni-Cr-H

Fig. 4. Lattice parameters of Ni-Cr hydride phases obtained at 2.7 GPa(H_2) and 298 K.
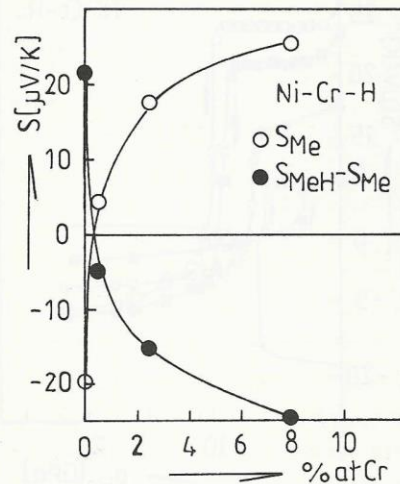
Fig. 5. Thermopower S and change of S during hydride formation as functions of Cr content in Ni-Cr alloys.

Nickel alloyed with *3d* elements; Hydrides formation

S.M. Filipek, H.J. Bauer, S. Majchrzak and H. Yamamoto, *Z. Phys. Chemie NF.*, **163 (1989)** 485.

or Pd-Ti do not differ much from that of pure palladium. The VBS of 3d transition metal impurities in palladium hydride has been discussed by Friedel /5/ and Daniel /6/, but without considering changes of hydrogen concentration within the β-hydride phase. A similar problem was studied in details for the Pd-Ru-H system by Wicke et al./7,8/ who reported the appearance of hydrogen induced magnetic moments localized on ruthenium for certain ranges of hydrogen concentrations in Pd-Ru alloys. The model proposed to explain this experimental result is shown in Fig. 1. Magnetic moments on ruthenium give rise to Kondo minima in the temperature dependence of the electrical resistivity /9/. Let us remark that a similar phenomenon has been observed for such nickel based VBS alloys as Ni-Cr /10/ and Ni-V /11/, hydrogenated using high pressure technique. In the case of Cr-rich Ni-Cr-H alloys Kondo type minima were found at unusually high temperatures /10/.

In this work the thermoelectric power, which is a property very sensitive to changes in the electronic structure in the vicinity of the Fermi level, has been measured as a function of hydrogen pressure for several Ni based and Pd based alloys. A similar behaviour has been observed for
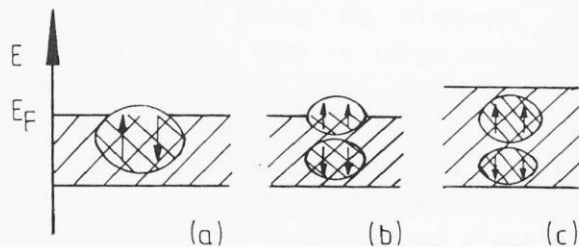

Fig. 1. A model describing the appearance of localized magnetic moments (LMM) in the (Pd-Ru)-H system. a) Virtual bound states of ruthenium in H-free palladium. b) Spin splitted VBS in β-PdH$_n$ at the low n limit. The Fermi level crosses the spin up sublevel giving rise to the LMM due to uncompensated spins. c) Further increase of hydrogen concentration results in a shift of the Fermi level above the upper limit of the splitted VBS. In consequence the LMM disappear. (According to Wicke et al./7,8/).

Local disturbances in the Electron Liquid; Virtual levels

A virtual bound level is a region of space and Energy around a foreign ion in a metal in which itinerant electrons linger and temporarily assume to a marked degree the atomic features of the precursor atomic state. Physically, the virtual level is formed from a resonance (hybridization) between the Energy level of an outer orbital of foreign atom and those levels in the host's conduction band that have comparable energy.

J. Hurd, *Electrons in metals* 1975

Virtual levels and hydride formation

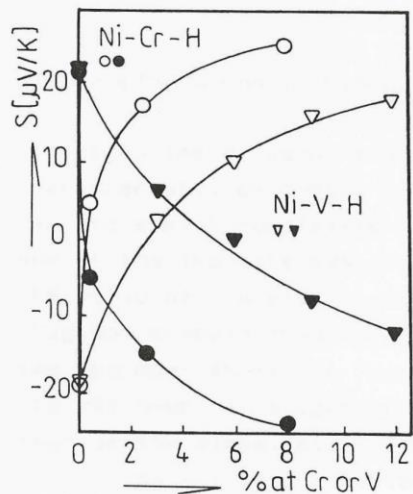A.W. Szafrański, S.M. Filipek, *Z.Phys. Chem. (N.F.)* **147 (1986)** 15

Fig. 2. Thermopower S_{Me} (open symbols) and change of thermopower ΔS during hydride formation (black symbols) as functions of Cr or V content in their nickel alloys.
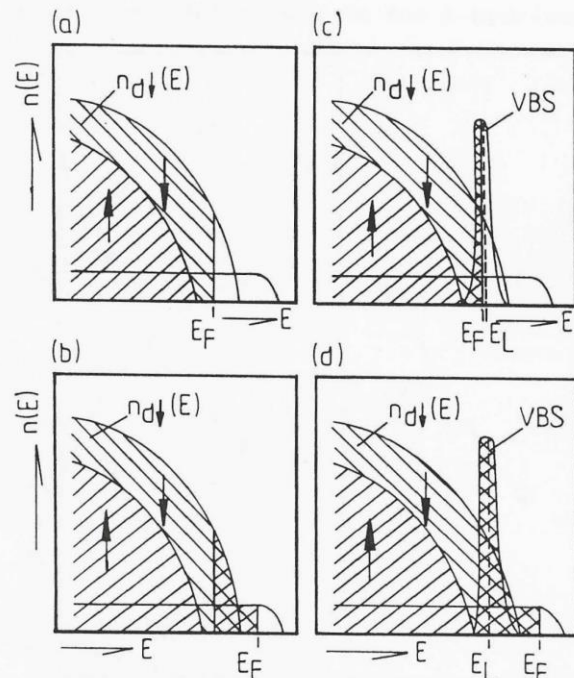

Fig. 3. Schematic view illustrating the band structure changes during hydride formation in pure Ni and in a nickel alloy in which a VBS is present at the Fermi level.

a) pure nickel
b) nickel hydride
c) H-free VBS alloy
d) hydride phase of this VBS alloy.

value of the nickel hydride. This behaviour can be qualitatively explained using a schematic model shown in Fig. 3. When nickel (Fig. 3a) transforms into Ni-hydride (Fig. 3b) the electrons introduced by the hydrogen fill up the empty

Nickel alloyed with *p* and *3d* elements;

Hydrides formation

S.M. Filipek, *Z. Phys. Chemie NF.*, **163 (1989)** 627.

Hydrogen in amorphous alloys

A consistent interpretation of the results is given within the framework of a Fermi-Dirac statistics, developed and used recently for the interaction of hydrogen with defects in solids. Equivalent to electrons in metals, hydrogen is distributed among sites of different energy caused by the disorder in an amorphous metal. By assuming a gaussian distribution of site energies for an amorphous metal it was shown by Kirchheim (j. Non-Cryst. Solids, 70 (1985) 23) that the chemical potential of hydrogen should be related to the hydrogen concentration by the following equation:

$$\mu = E' + \sigma \text{ inverf } (1 - 2c)$$

Where σ is the width and E' the everage energy of the gaussian distribution

Hydrogen in amorphous alloys
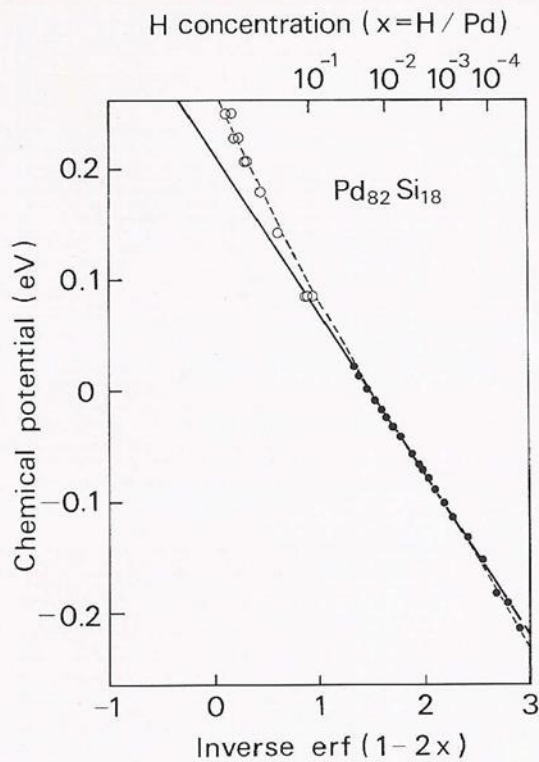
Chemical potential of hydrogen in amorphous Pd82Si18 at 295 K vs. inverse error function erf /1 – 2x/. The dotted line corresponds to a chemical potential which contains H-H interaction term 0,12 x eV per hydrogen atom.

4. CONCLUSIONS

It has been shown that the measured activity of hydrogen in amorphous Pd–Si alloys can be described with the following assumptions:

(1) Hydrogen is dissolved in a solid matrix with a spectrum of different sites or a spectrum of binding energies, respectively, where the thermal occupancy of the sites is given by Fermi–Dirac statistics.

(2) A Gaussian function is an appropriate distribution function of site energies to describe hydrogen activity over eighteen orders of magnitude.

(3) Deviations from this theoretical treatment occur at concentrations of $H/Pd > 0.1$ and can be interpreted either by a repulsive H–H interaction energy within the framework of a quasichemical approach or by a smaller number of available interstices in the amorphous structure in comparison with crystalline Pd.

SEARCH FOR "COLD-FUSION" IN SOME Me–D SYSTEMS AT HIGH PRESSURES OF GASEOUS DEUTERIUM*

B. BARANOWSKI and S. M. FILIPEK

Institute of Physical Chemistry, Polish Academy of Sciences, 01-224 Warsaw (Poland)

M. SZUSTAKOWSKI, J. FARNY and W. WORYNA

Institute of Plasma Physics and Laser Microfusion, 00-908 Warsaw, P.O. Box 49 (Poland)

Summary

Metallic palladium and nickel were treated with gaseous deuterium at 298 K to pressures of 3.1 GPa and 1.0 GPa respectively. The high concentrated deuterides did not exhibit, at long time equilibrium as well as in dynamic conditions, evidence of neutron emission nor evolution of heat due to possible "cold fusion". The volume concentrations of deuterium definitely exceeded those achieved by electrolytic charging. Electrical resistance measurements of palladium deuteride up to 3.1 GPa of gaseous deuterium indicated a further uptake of deuterium above the estimated stoichiometry of octahedral vacancies. A partial filling up of tetrahedral vacancies probably takes place. Electrolytic charging in high pressures of gaseous deuterium did not improve the negative observations above. Thus the observations of Fleischmann and Pons are not confirmed at higher volume concentrations of deuterium in the palladium and nickel lattice as well in equilibrium as in dynamic conditions (phase transitions, high pressure electrolysis).

1. Introduction

The recently published information about "cold fusion" in electrolytically prepared palladium deuteride [1] presents an attractive challenge for Me–D systems.

However, the electrochemical preparation used [1] has three disadvantages.

(1) The thermodynamically reversible range is rather limited and uninteresting for "cold fusion" purposes, but in the range of large overpotentials the activity of the electrode surface is hardly reproducible and stable. Thus results obtained at different places cannot be compared in an objective way and station-

---

*Results of this paper were presented on July 20 on the high pressure conference (AIRAPT) in Padeborn (F.R.G.).
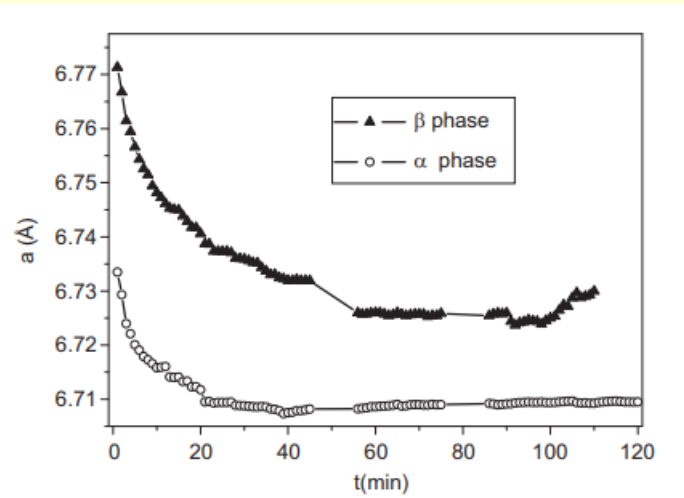
Fig. 4. Time dependence of lattice parameters of α and β phases of ZrNi$_5$H$_x$ sample calculated from data given in Fig. 2.
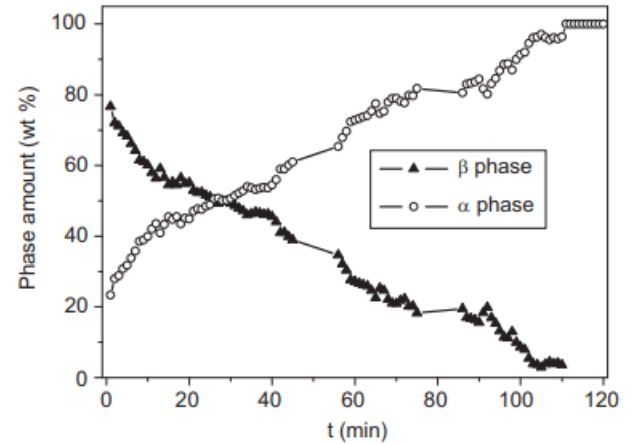

Fig. 5. Time dependent of weight percent of α and β phases of ZrNi$_5$H$_x$ sample calculated from data given in Fig. 2.

Table 1
Comparison of hydrogen absorption in Zr–Ni based alloys performed in different conditions.

Sample	Lattice parameter [Å]	Unit cell volume [Å^3]	Volume expansion/f.u. $\Delta V/Z$ [Å^3]	Calculated hydrogen content H/f.u.	Conditions of treatment
Parent ZrNi$_5$	6.7030	301.167			
α$_0$-phase	6.7335(7)	305.293	1.03	0.38	
α$_{100}$-phase	6.7092(3)	302.000	0.21	0.08	After treatment at 0.9 GPa(H$_2$)
β$_0$-phase	6.7713(3)	310.463	2.324	0.86	
ZrNi$_5$	6.7027(3)	301.131			
ZrNi$_5$H$_{0.5}$				0.5	
La$_{0.5}$Zr$_{0.5}$Ni$_5$ (by ball milling)	$a = 4.8704$ $c = 4.0293$	82.77			Treatment at 10 MPa (H$_2$) Ref.[6]
La$_{0.5}$Zr$_{0.5}$Ni$_5$H$_{1.12}$				1.12	
ZrNi$_5$	6.683	298.5			Treatment at 2.5 MPa (H$_2$) Ref. [4]
ZrNi$_5$H$_{0.57}$	6.707	299.8	0.76	0.57 (0.28)	
ZrNi$_{4.8}$Al$_{0.2}$				0.005	By cathodic charging; Ref. [5]
Zr$_9$Ni$_{91}$	2.851 (bcc)				
Zr$_9$Ni$_{91}$H$_{52}$				0.52[a]	Treatment at 700 MPa. Ref. [12]
Zr$_9$Ni$_{91}$H$_{39}$	Amorphous			0.39[a]	

[a] H/M.

Manganese hydrides

The Fig.1 represents results plotted in the T - p(H_2) diagram together with previous data.

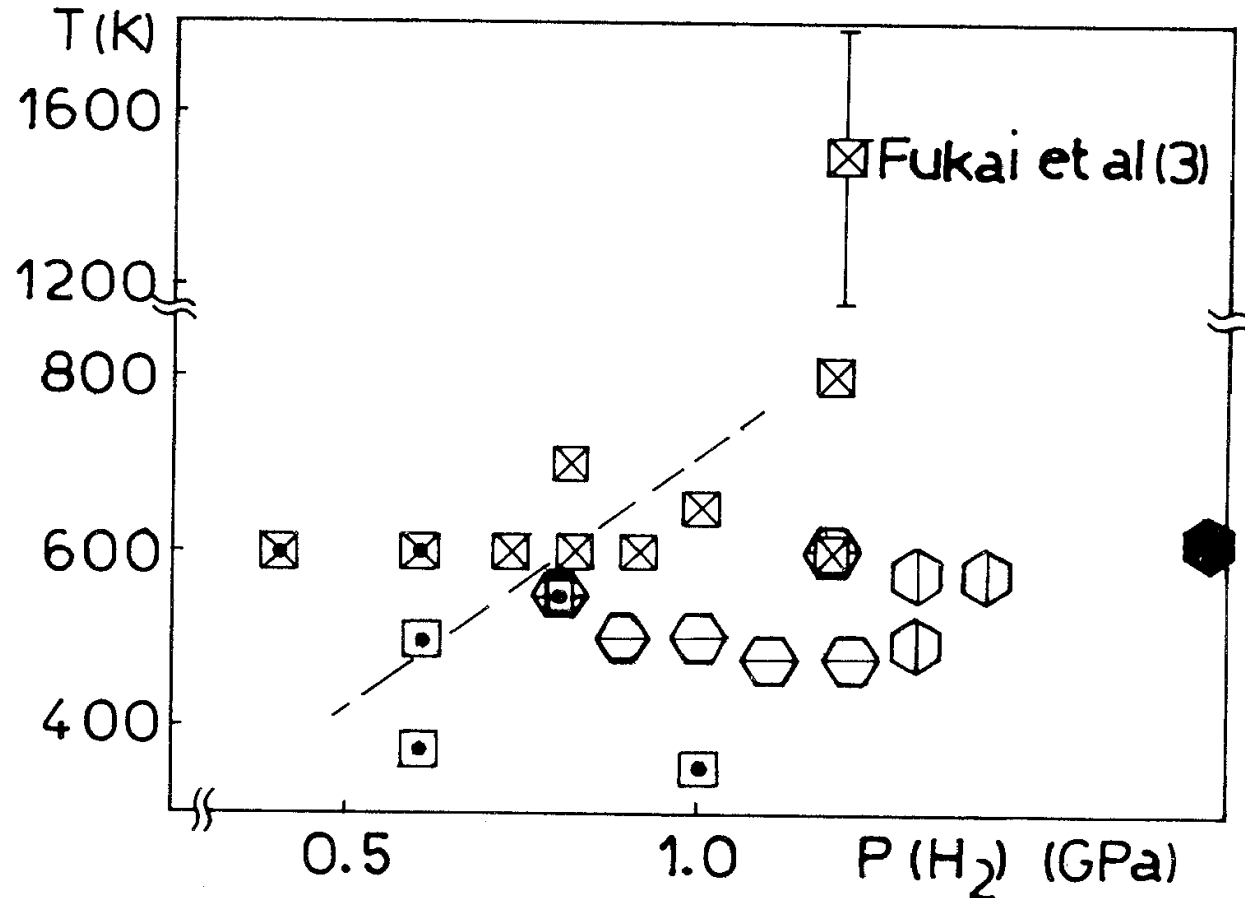Fig.1. Results of X-ray analysis plotted on the T - p(H_2) diagram. $\boxdot$ αMn; $\boxtimes$ fccMnH$_x$; $\ominus$ hcpMnH$_x$; $\boxtimes$ αMn+fccMnH$_x$; $\ominus$ αMn+hcpMnH$_x$ $\otimes$(fcc+hcp)MnH$_x$ (our results). $\ominus$ hcpMnH$_x$ (Ref.1). --- onset of the hcpMnH$_x$ formation, $\blacksquare$ hcpMnH$_x$ (Ref.2).

S.M. Filipek, S. Majchrzak, A.B. Sawaoka, M. Cernansky, *High Press. Res.* **7**, 271 (**1991**).

Sample 1 hcp $MnH_{0.84}$	1.0 GPa (H_2) and 500 K (during 48 hours)	(a=2.700 Å, c=4.378 Å)
Sample 2 fcc $MnH_{0.64}$	1.2 GPa (H_2) and 800 K during 72 hours	non Ferromagnetic (a=3.827 Å)
Sample 3 fcc $MnH_{0.30}N_{0.08}$	1.0 GPa (H_2) and 600 K (during 50 hours). The small amount of nitrogen was added to the hydrogen gas.	Ferromagnetic (a=3.856 Å)
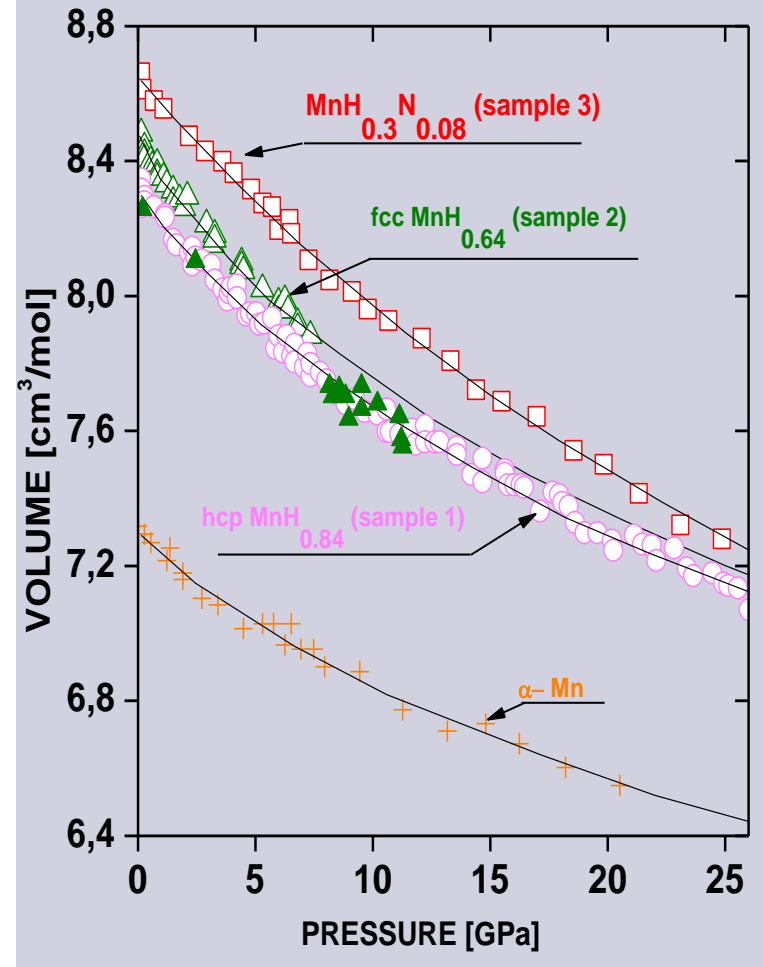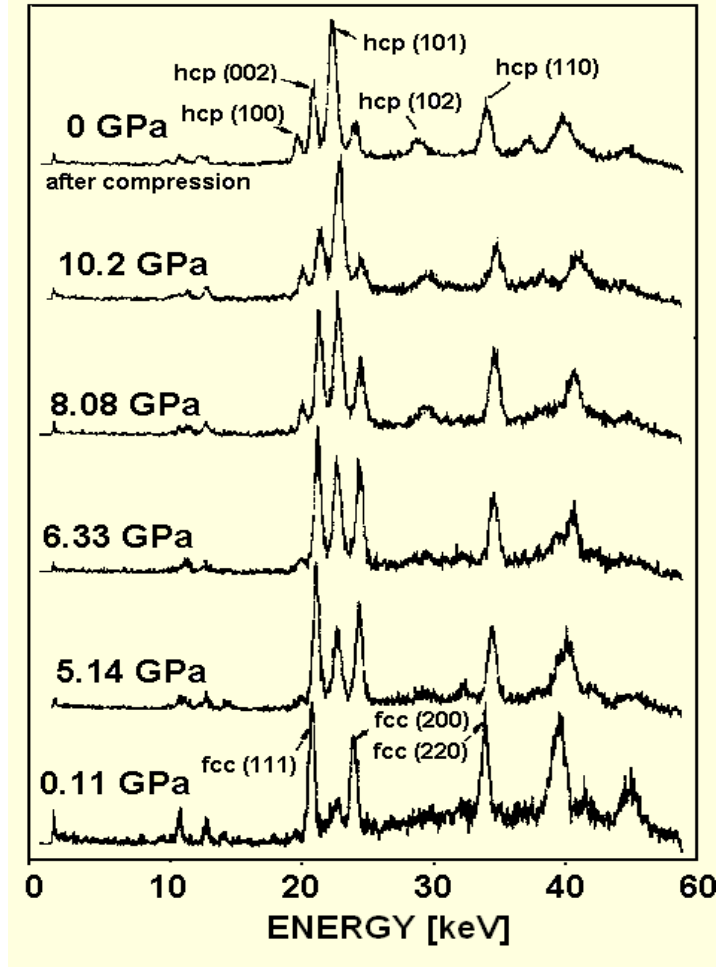
X-ray diffraction pattern for fcc- MnH$_{0.64}$ (sample 2) observed during the in situ measurements in DAC aparatus

Compression curves of manganese hydrides. For sample 2 the closed symbols correspond to reduction of pressure. For other samples data for pressure increase and reduction did not differ.

S.M. Filipek, H. Sugiura, T. Skoskiewicz: AIRAPT-17 Proc. Science and Technology of High Pressure (Murli H. Manghnani, William J. Nellis and Malcolm F. Nicol Eds.) Universities Press, Hyderabad, India **2000** p. 550-554.

Influence of hydrostatic pressure on $MnH_{0.64}$ and $MnH_{0.30}N_{0.08}$ samples

fcc $MnH_{0.64}$
non
ferromagnetic
(a=3.827 Å)

→ *irreversible pressure induced phase transition* → hcp $MnH_{0.64}$

hcp $MnH_{0.84}$
(a=2.700 Å,
c=4.378 Å)

→ *compression up to 30 GPa* → no structural changes

fcc $MnH_{0.30}N_{0.08}$
Ferromagnetic
(a=3.856 Å)

→ *pressure up to 30 GPa* → no structural changes

↓ *Evacuation of hydrogen at 250°C*

fcc
Ferromagnetic

→ *transformation around 8 GPa* → α-Mn

S.M. Filipek, H. Sugiura, T. Skoskiewicz: AIRAPT-17 Proc. Science and Technology of High Pressure (Murli H. Manghnani, William J. Nellis and Malcolm F. Nicol Eds.) Universities Press, Hyderabad, India **2000** p. 550-554.

Aluminum hydride

AlH_3 can be synthesized in a reaction between lithium aluminum hydride and aluminum chlodride carried out in an organic solvent. Formation of AlH_3 from elements required pressure higher than 2.8 GPa(H_2) and temperature T = 573 K.

M. Tkacz, S.M. Filipek, B. Baranowski, *Polish J.Chem.*, **57 (1984)** 651.

Baranowski, B.; Tkacz, M.; Filipek, S. High pressure investigations of the Al-H system. Mater. Res. Soc. Symp. Proc. 1984,22, 53–56.

Studies of Laves Phase Hydrides

➢ Introduction and Experimental Techniques.

➢ Novel Laves phase hydrides synthesized under high hydrogen pressure;

- Simple lattice expansion case ($ZrFe_2H_4$, $ZrCo_2H_2$)

- Derived by expansion and distortion of the parent lattice ($ErFe_2H_5$, YFe_2H_5)

- Derived by the total restructurization of the parent lattice (YMn_2D_6, $ErMn_2D_6$, $DyMn_2D_6$ and $HoMn_2D_6$)

  Never observed before in Laves-based hydrides

➢ Selected properties of novel RMn_2D_6 hydrides.

➢ Studies under high hydrostatic pressures.

➢ Summary and Conclusions

Laves phases

➢ In recent decades, a large number of intermetallic compounds have been synthesized and their properties have been studied. Among them AB_2 Laves phases attract especially great interest due to their physical properties and possible practical applications. These phases can be formed from various elements of different groups of the Periodic Table. For instance they can contain Y, Zr or Rare - earth and a transition metal.

➢ The Laves AB_2 compounds can crystallize in three structures: cubic - C15 (MgCu2) and two hexagonal - C14 (MgZn2) and C36 (MgNi2).
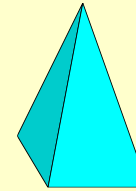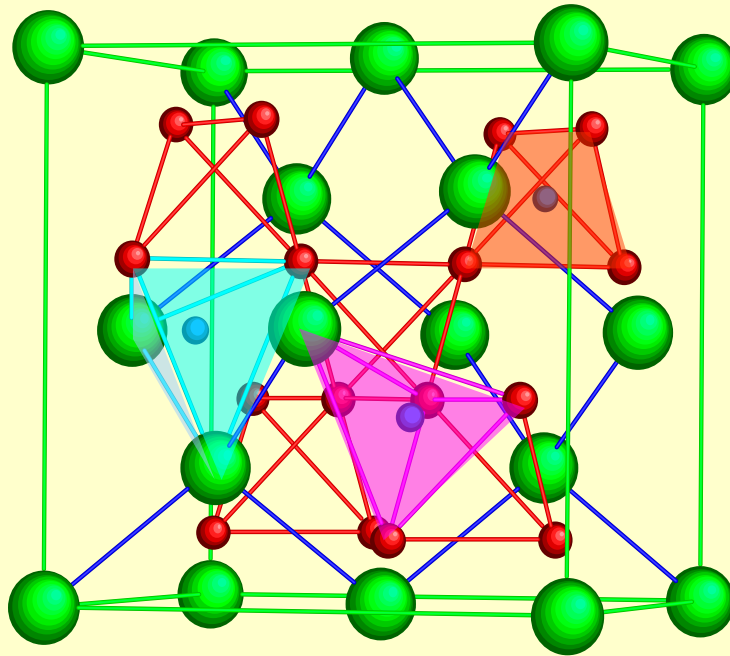
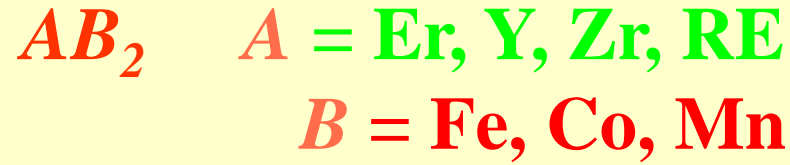# Laves intermetallics RT$_2$
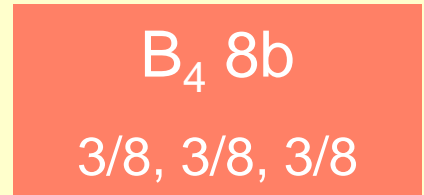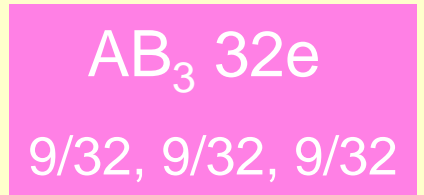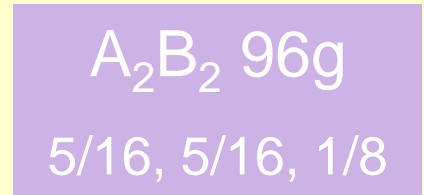## C15 (*Fd3m*)   C14 (P6$_3$/mmc)
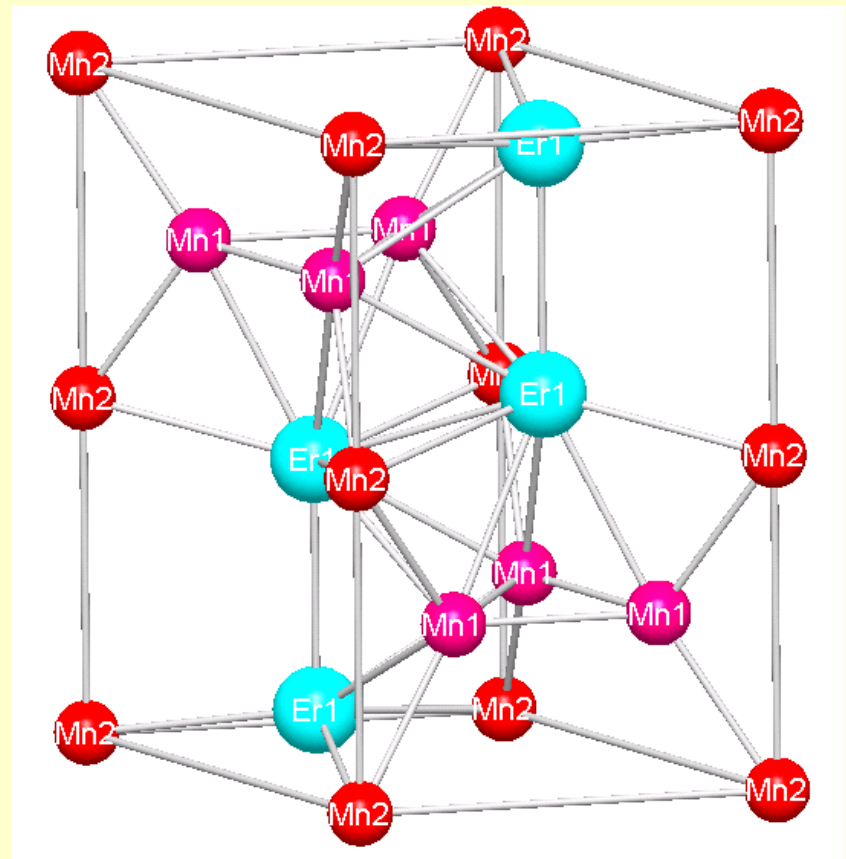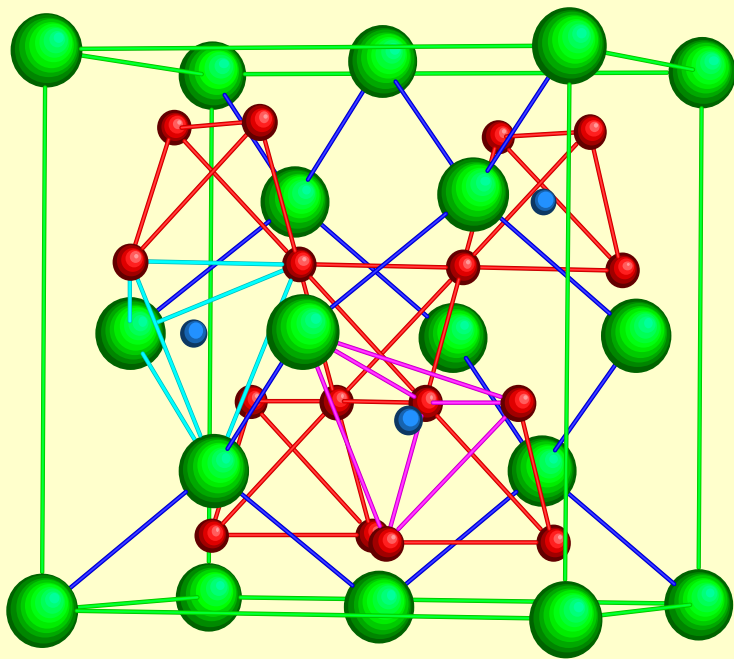
Laves – Hydrogen absorption

➢ Hydrogen absorption in intermetallic compounds of rare earth and transition metal has raised interest in both fundamental and application field (H storage, batteries...).

➢ In RT_2 compounds, hydrogen absorption leads to the formation of several single-phase hydrides, which crystallize in different structures, derived from that of the parent compound. The lowering of the crystal symmetry has been related to hydrogen ordering in preferential interstitial sites.

➢ In all the RT_2 hydrides the modification of the crystal structure accompanied by an increase of the cell volume, leads to a change of the magnetic properties. The increase of the T-T distances and the change of the atomic bounds, due to various H surrounding explain this evolution.

LAVES phases

AB_2 A = Er, Y, Zr, RE

B = Fe, Co, Mn

A

B

H

H sites:

A_2B_2 96g
5/16, 5/16, 1/8

AB_3 32e
9/32, 9/32, 9/32

B_4 8b
3/8, 3/8, 3/8

The crystal structure of
C15 Laves phase

XRD and NPD measurements

- The X-ray diffraction (XRD) patterns were measured with a D8 Brucker diffractometer equipped with a rear graphite monochromator in the range $10°< 2\theta < 120°$ with a step of $0.02°$ using Cu Kα radiation.

- The neutron powder diffraction (NPD) patterns of the deuteride have been registered at 2 K and 80 K on the 3T2 diffractometer and at 1.5 K, 80 K and 290 K on the G4.1 diffractometer at the Laboratoire Léon Brillouin (LLB) at Saclay. For the 3T2 experiment the wavelength was 1.225 Å and the angular range $6° < 2 < 125°$ with a step of $0.05°$. For the G4.1 experiments the wavelength was 2.427 Å and the angular range was $2° < 2 < 82°$ with a step of $0.1°$. The deuteride sample was contained in a vanadium sample holder. All the XRD and NPD patterns were refined with the Rietveld method, using the Fullprof code. The line shapes were refined with a Pearson VII function.

Synchrotron Measurements

➢ Synchrotron XRD experiments were carried out in the BL 01C2 beam line (National Synchrotron Radiation Research Center (NSRRC), Taiwan) by using a DCM monochromator with a wavelength of synchrotron radiation 1.3332Å. Structural refinements were made with X-ray data by using GSAS program.

➢ The Mn and Fe K-edge XANES measurements were recorded in absorption mode for synthesized alloys and their hydride mounted on a scotch tape, at BL 17C Wiggler beam line (NSRRC) using a double-crystal Si (111) monochromator. The X-ray harmonic was rejected by mirrors. The ion chambers used for measuring the incident (I0) and transmitted (I) beam intensities were filled with a mixture of N2 and H2 gases and a mixture of N2 and Ar gases, respectively. Energy calibration was carried out by using the first inflection point of the spectrum of Mn and Fe metal foils as references (Mn K-edge: 6539 eV and Fe K-edge: 7112 eV). Reference spectra were simultaneously collected for each in situ spectrum by using Mn and Fe metal foils.

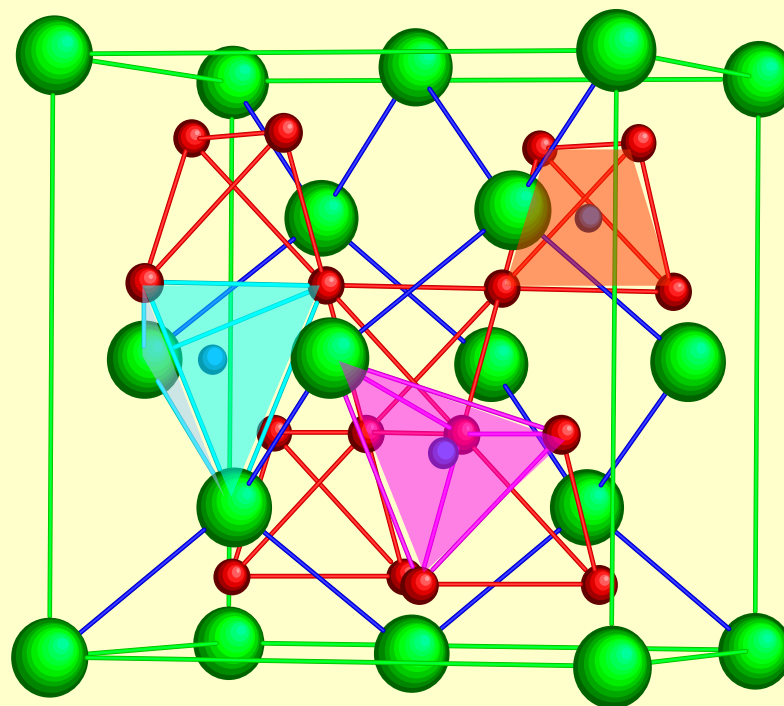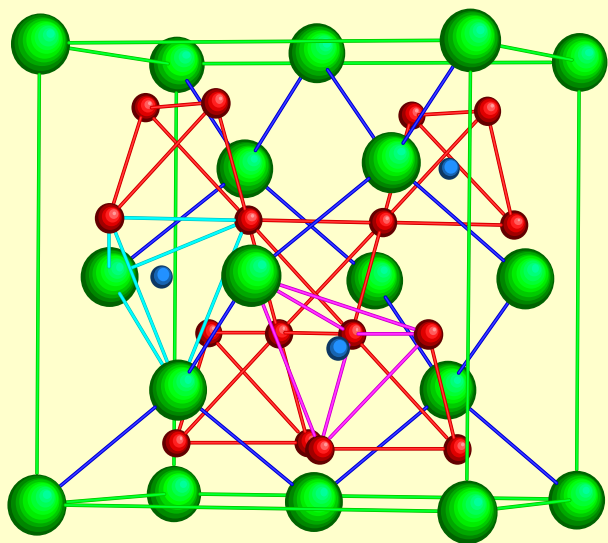# Hydrides formed by simple lattice expansion ($ZrFe_2H_4$, $ZrCo_2H_2$)

ZrFe$_2$ - H$_2$ system   XeD

ZrFe$_2$ - H$_2$ system   **XRD**
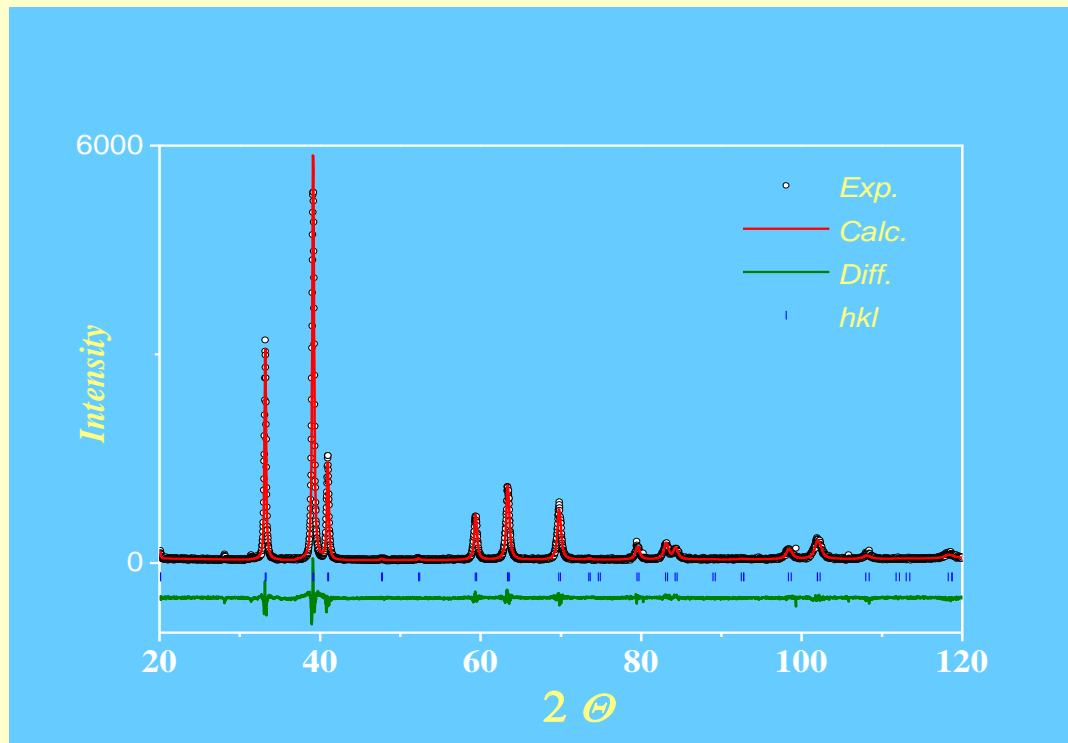
P(H$_2$)=0.35 GPa

T = 100°C

Compound	Space group	a (Å)	V, Å³	ΔV/V (%)
ZrFe$_2$	Cubic (Fd3m)	7.072	354	-
ZrFe$_2$H$_4$	Cubic (Fd3m)	7.637	445	26

S. M. Filipek, I. Jacob, V. Paul-Boncour, A. Percheron-Guegan, I. Marchuk, D. Mogilyanski, J. Pielaszek: *Polish J. Chem.,* **75** 12), **(2001)**, 1921-1926.

ZrFe$_2$ or ZrCo$_2$
C15 (*Fd3m*) $\longrightarrow$ C15 (*Fd3m*)

S. M. Filipek, I. Jacob, V. Paul-Boncour, A. Percheron-Guegan, I. Marchuk, D. Mogilyanski, J. Pielaszek: *Polish J. Chem.,* **75**, (12), **(2001)**, 1921-1926.

$ZrFe_2H_4$
Magnetic measurements
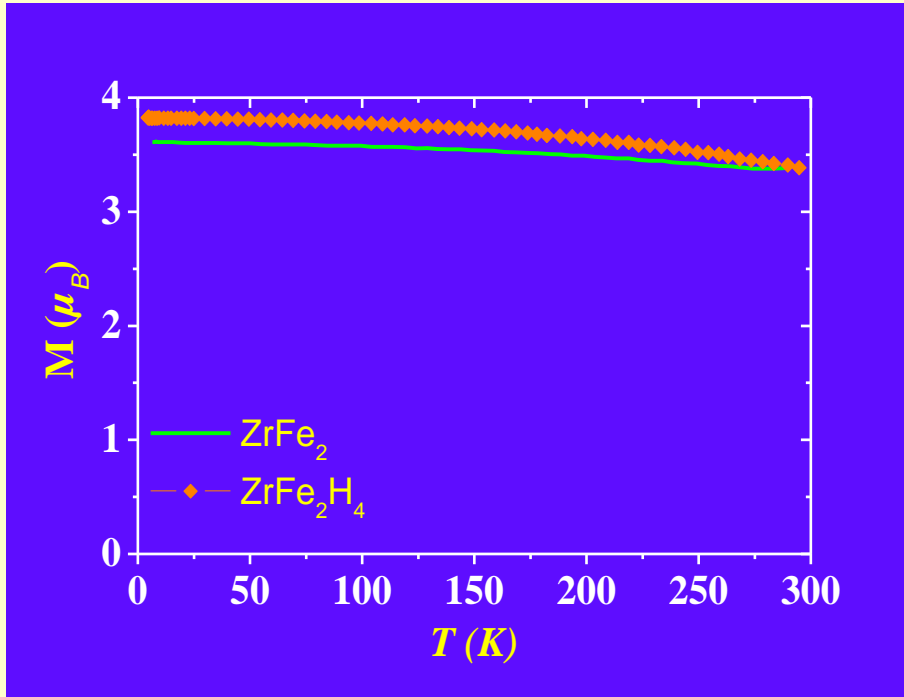
Thermomagnetization curves
of **$ZrFe_2$ and $ZrFe_2H_4$**
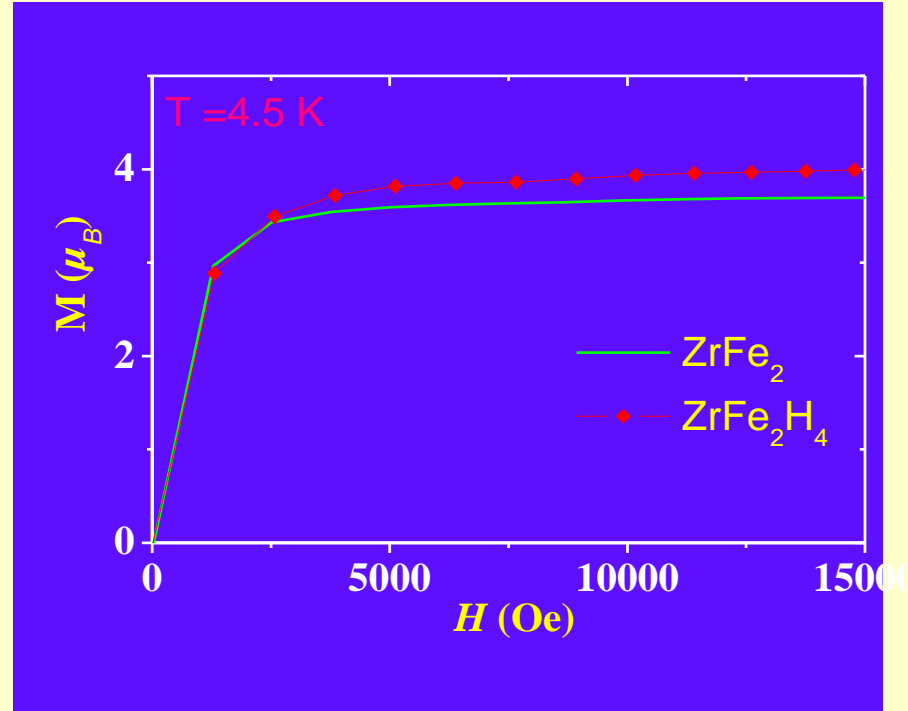
Magnetization curves
of **$ZrFe_2$ and $ZrFe_2H_4$**

$ZrFe_2$: Ms = **1.78** μ_B/Fe
$ZrFe_2H_4$: Ms = **1.88** μ_B/Fe

ZrFe$_2$ - D$_2$ system

RESULTS:

Refined ND pattern of a ZrFe$_2$D$_4$ (270 K)

12 % **ZrFe$_2$** $a = 7.062$ Å
Cubic *Fd3m*

88% **ZrFe$_2$D$_x$** $a = 7.564$ Å

Cubic *Fd3m*

$\Delta V/V = 22.8$ %

A$_2$B$_2$ and *AB$_3$*

x = 2.70 D/ZrFe$_2$

V. Paul-Boncour, F. Bouree-Vigneron, S.M. Filipek, I. Marchuk, I. Jacob, A. Percheron-Guegan, **356-357** (**2003**) 69

ZrCo₂ - H₂ system

XRD

$P(H_2) = 1.0\ GPa$

$T = 100^oC$

Compound	Space group	a (Å)	V, Å³	ΔV/V (%)
ZrCo₂	Cubic (Fd3m)	6.945	335	-
ZrCo₂H₂	Cubic (Fd3m)	7.267	384	14

V. Paul-Boncour, F. Bouree-Vigneron, S.M. Filipek, I. Marchuk, I. Jacob, A. Percheron-Guegan, J.Alloys and Comp.. **356-357** (**2003**)

ZrCo₂D₂

ND
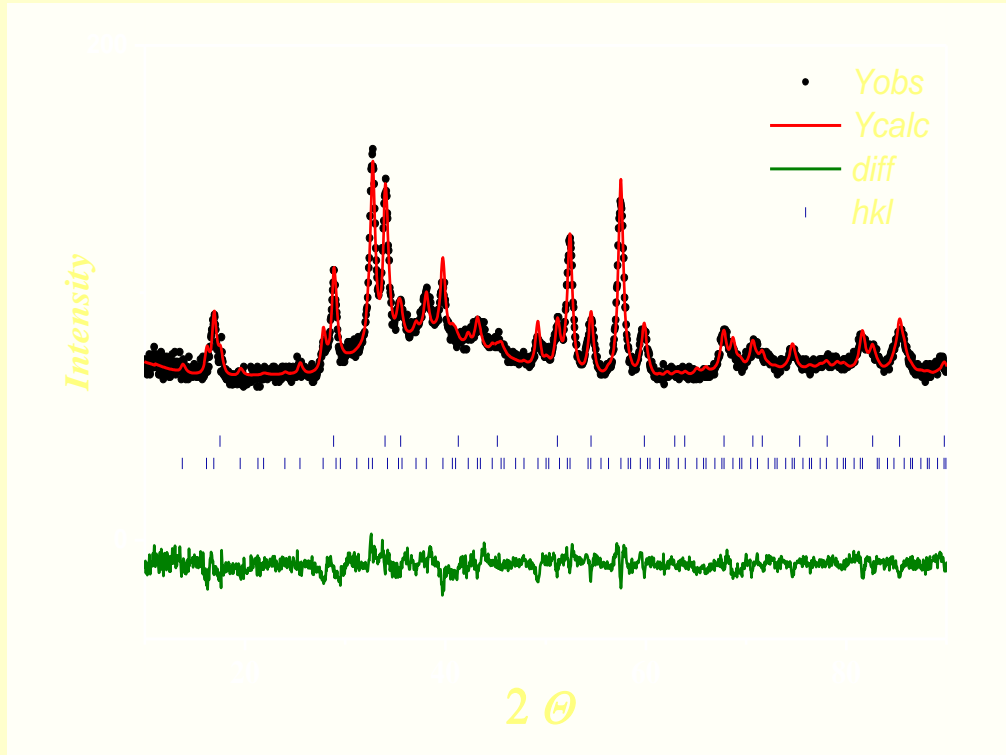
Refined ND pattern of a ZrCo₂D₂ (10 K)

RESULTS:

ZrCo₂ $a = 6.993$ Å
Cubic *Fd3m*

ZrCo₂D$_x$ $a = 7.191$ Å
Cubic *Fd3m*

ZrCo₂D$_x$
$a = 2 * 7.191 = 14.382$ Å
Cubic *F43m*

A₂B₂

$x = 1.65$ D/ZrCo₂

V. Paul-Boncour, F. Bouree-Vigneron, S.M. Filipek, I. Marchuk, I. Jacob, A. Percheron-Guegan, J. Alloys Comp. **356-357** (**2003**) 69
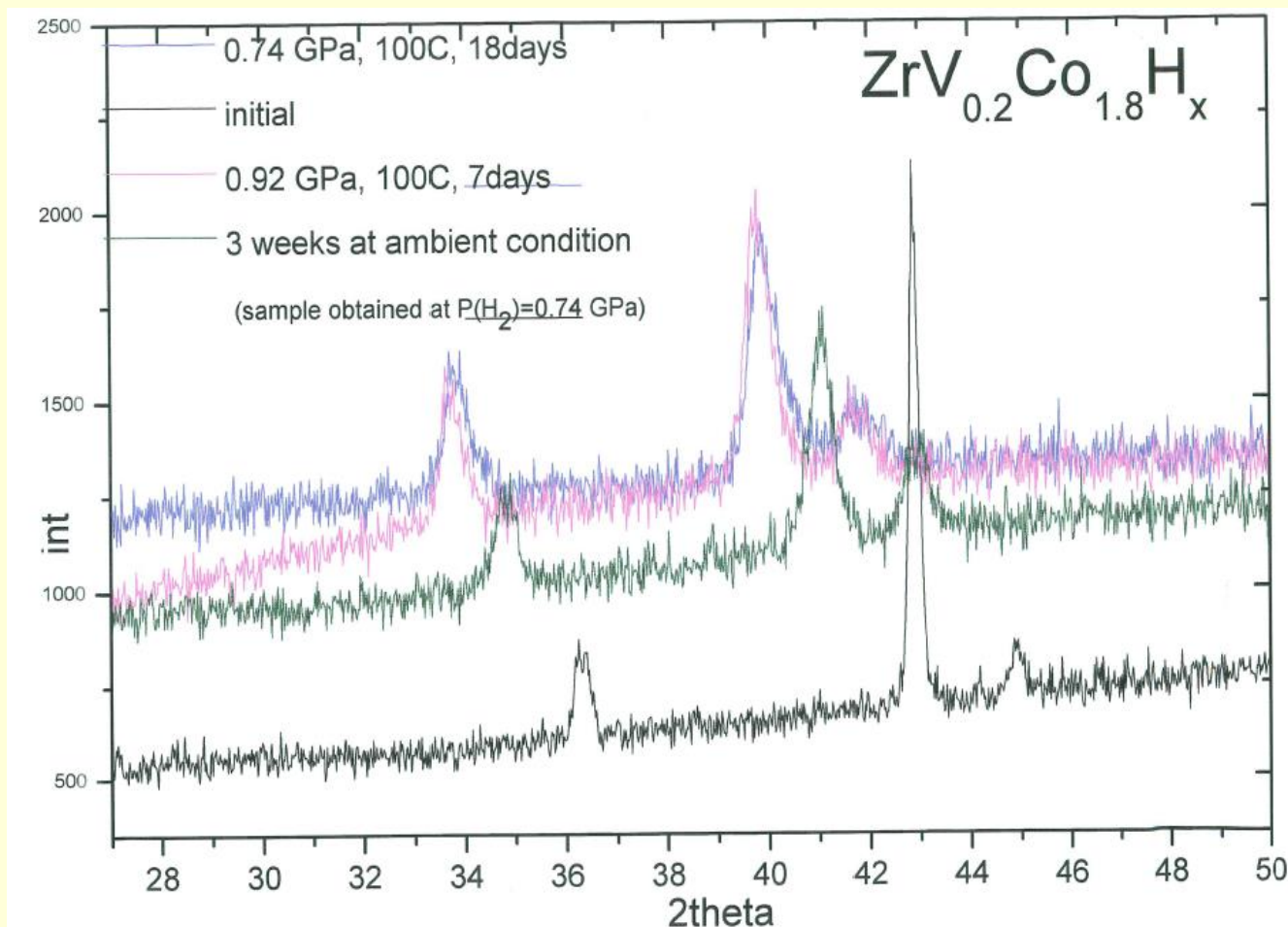
Stabilization effect of V addition

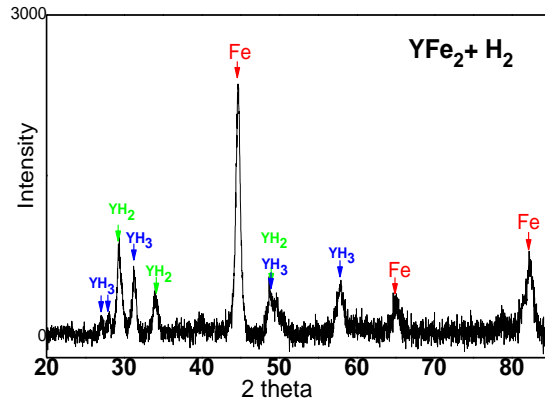*N. Takeichi, H. Tanaka, N. Kuriyama AIST*
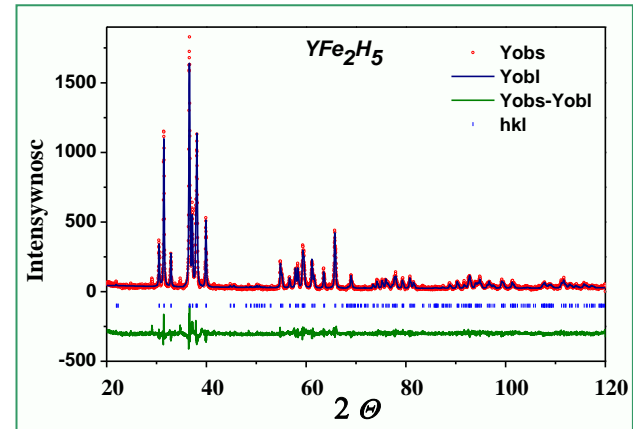*I. Marchuk, R. Sato S.M. Filipek – IPhChem. PAS*

Hydrides derived by expansion and distortion of the parent lattice ($ErFe_2H_5$, YFe_2H_5)
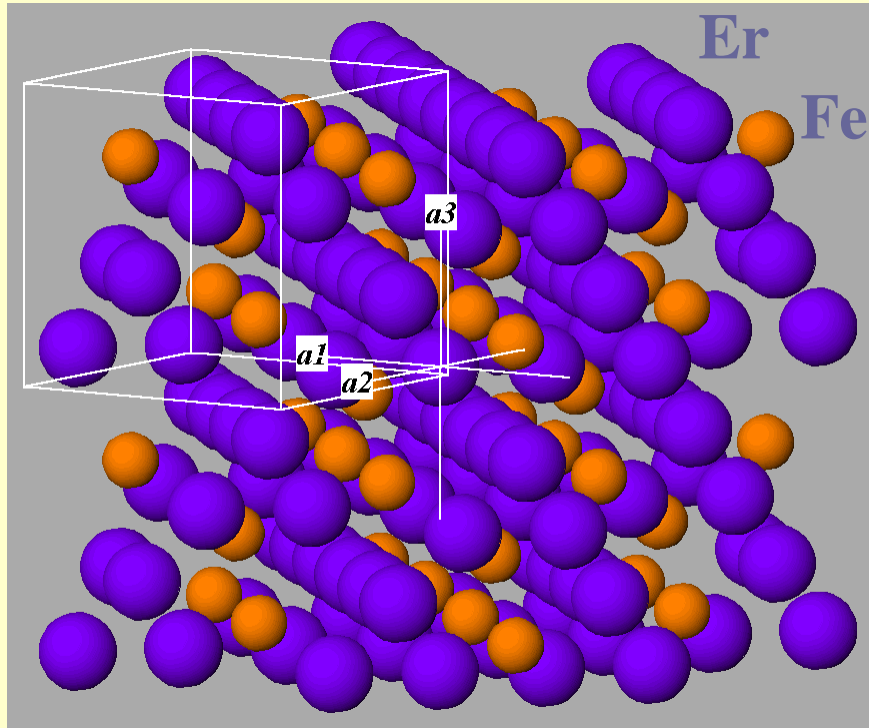
Synthesis of YFe_2H_5

a)

b)
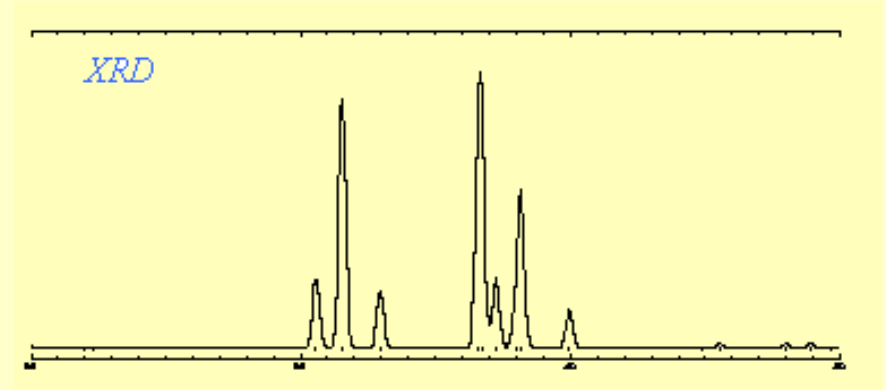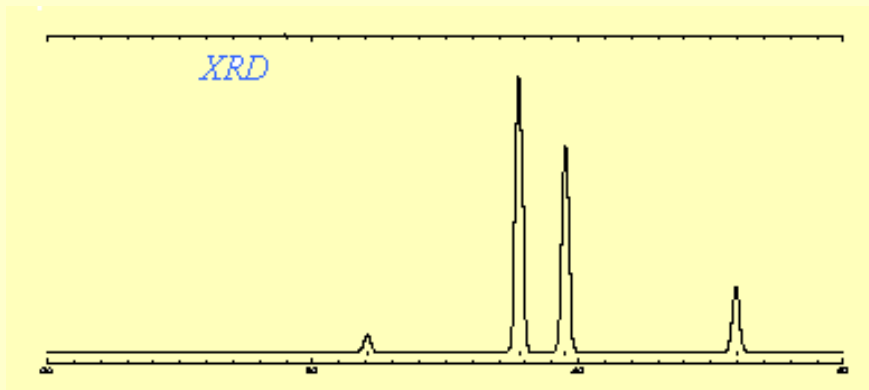

- Synthesis at 10 Kbar (H_2), 397 K, 7 days, but!!!

a) with rapid exposition, without cooling, to high hydrogen pressure – **SEGREGATION!**

b) appropriate hydrogenation resulted in synthesis of YFe_2H_5 – **SYNTHESIS OF NOVEL HYDRIDE!!**

V. Paul-Boncour, S.M. Filipek, A. Percheron-Guegan, I. Marchuk, J. Pielaszek: *Journ. Alloys Comp.*, **317-318** (**2001**) 83-87.

YFe$_2$/ErFe$_2$ (Cubic Fd3m)   YFe$_2$H$_5$ (Orthorhombic *Imm2*)
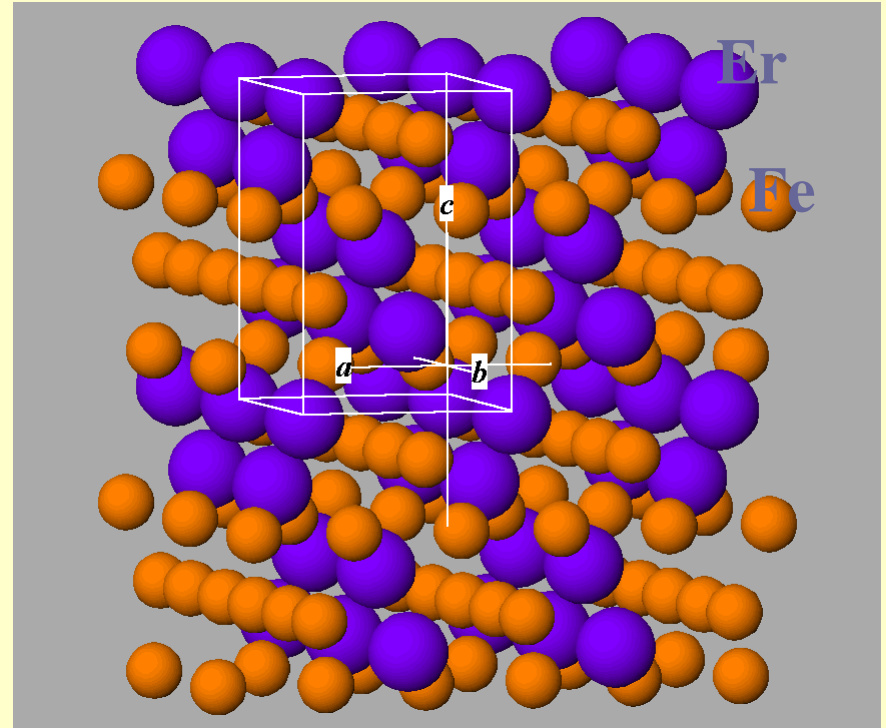
K. Shashikala, P. Raj, A. Sathyamoorthy, Mat. Res. Bull., 31, (1996), 957 .

Paul-Boncour V, Filipek S M, Marchuk I, André G, Bourée F, Wiesinger G, Percheron-Guégan A. J. Phys.:Cond. Matt. 2003; 15: 4349-59

YFe_2H_5

XRD
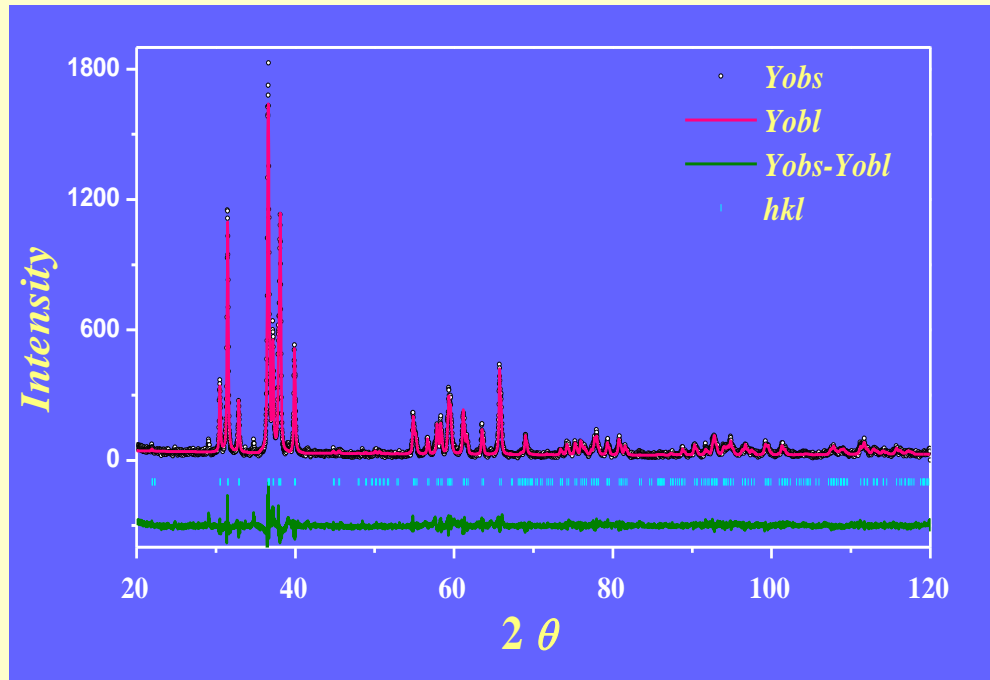
Compound	Space group	Lattice parameters (Å)			$V, Å^3$
		a	b	c	
YFe_2	Cubic *(Fd3m)*	7.36	-	-	398
YFe_2H_5	Orthorhombic*(Imm2)*	5.437	5.850	8.083	257

YFe_2H_5

Magnetic measurements

YFe_2 $M= 2.9\ \mu_B/YFe_2$
YFe_2H_5 $M_s= 0.8\ \mu_B/YFe_2$
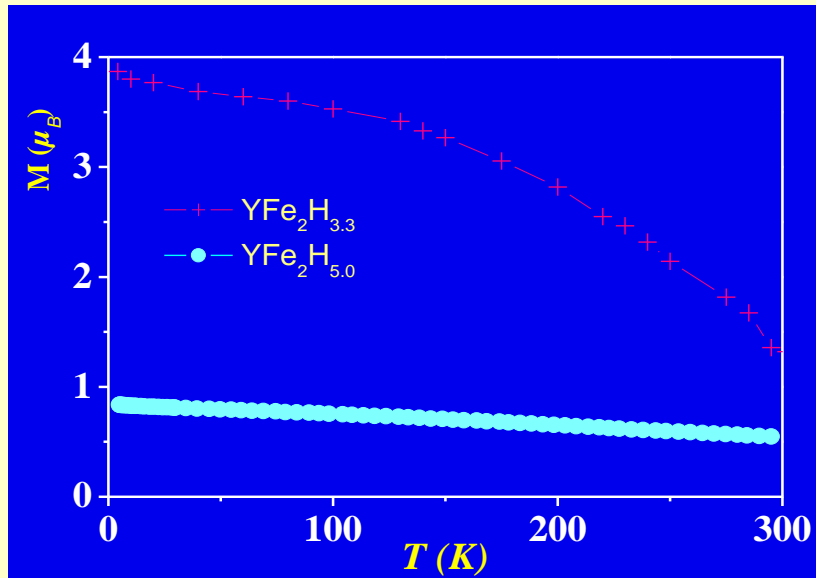
Temperature dependant
magnetization of YFe_2H_x compounds
for x= 3.3 and 5 H/f.u.)
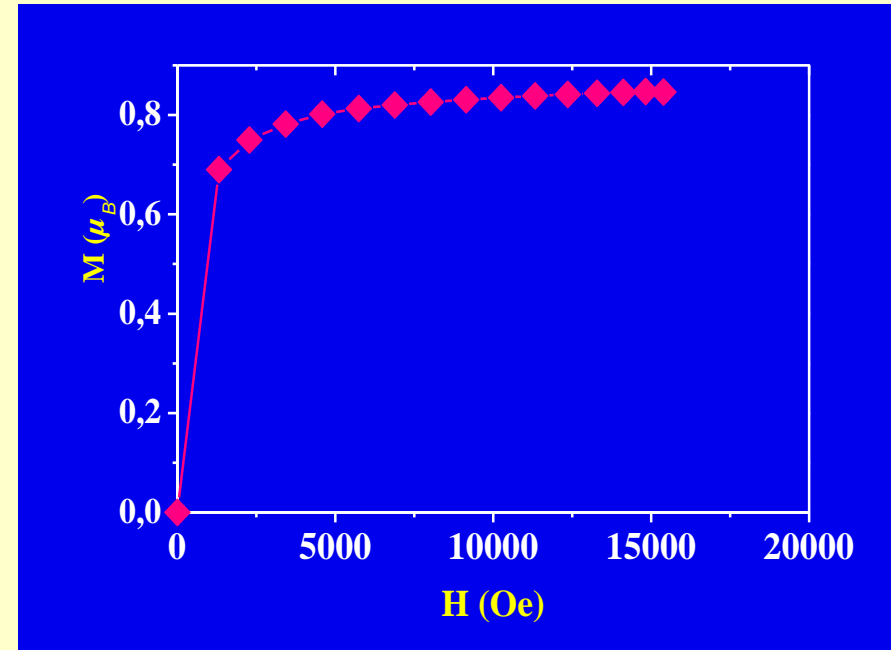
Magnetization versus fields of YFe_2H_5
(T=6K)

V. Paul-Boncour, S.M. Filipek, A. Percheron-Guegan, I. Marchuk, J. Pielaszek: *Journ. Alloys Comp.*, **317-318** (**2001**) 83
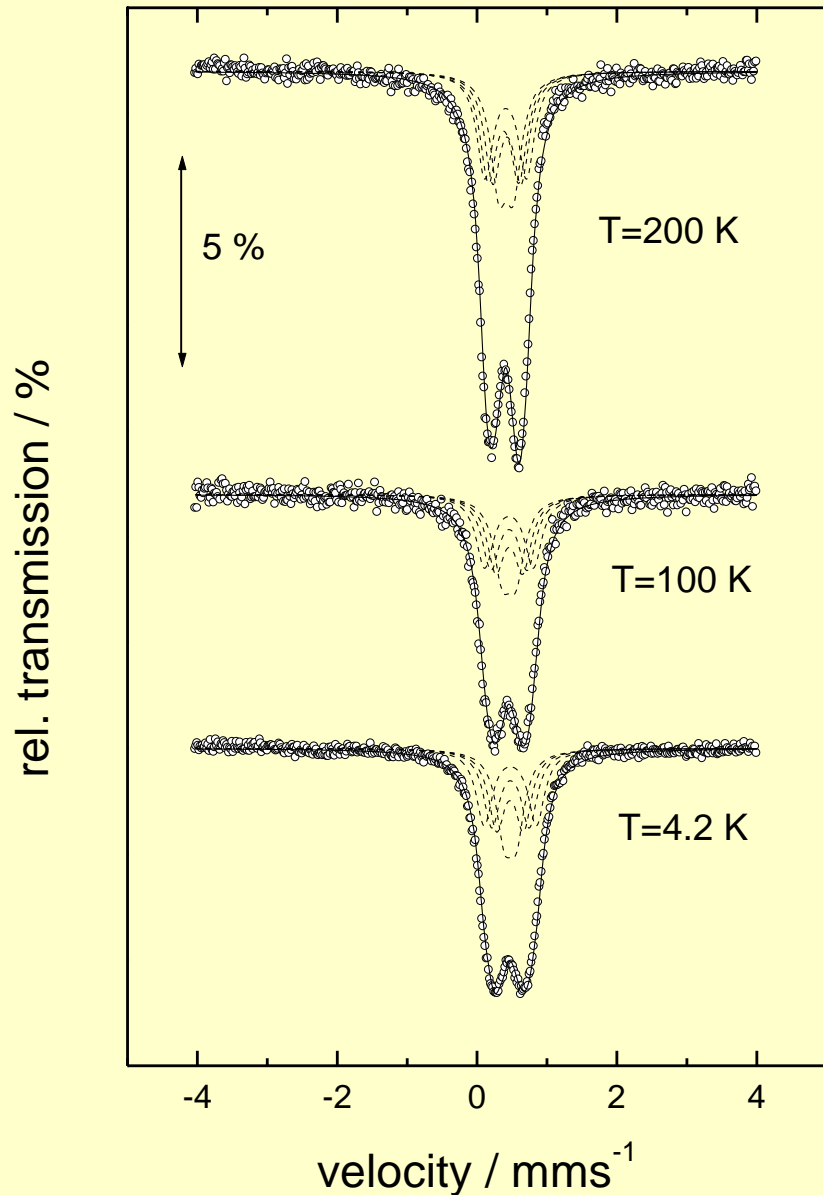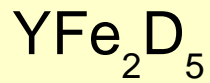
YFe$_2$D$_5$

Mössbauer spectrum
recorded from YFe$_2$D$_5$ at
various temperatures;
O - experimental points;
Solid line - total spectrum.

ErFe$_2$D$_5$

Neutron diffraction
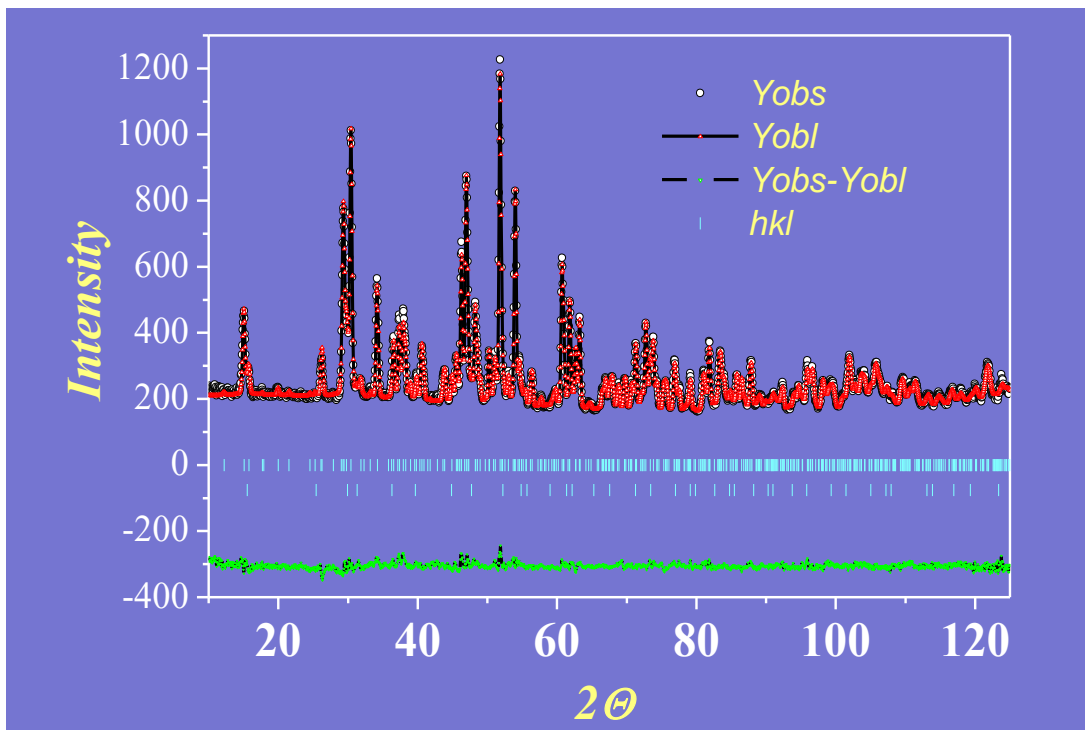
Refined ND pattern of a ErFe$_2$D$_5$ compound measured on the 3T2 spectrometer at 270 K.

Results:

3.8 % ErFe$_2$D$_4$
a = 7.781 Å
Cubic (Fd3m)

96.2% ErFe$_2$D$_5$
a = 5.418 Å, *b* = 5.732 Å,
c = 7.936 Å
orthorhombic (Pmn21)

A$_2$B$_2$ and AB$_3$

4.62 D/ErFe$_2$

V. Paul-Boncour, S.M. Filipek, I. Marchuk, G. Andre, F. Bouree, G. Wiesinger, A. Percheron-Guegan, J.Phys.; Condens. Matter **15 (2003)** 4349

YMn$_2$D$_6$
Hydride derived by the total restructurization of the parent lattice
Never observed before in Laves - hydrogen systems

YMn$_2$ (C15 Laves) and YMn$_2$D$_6$
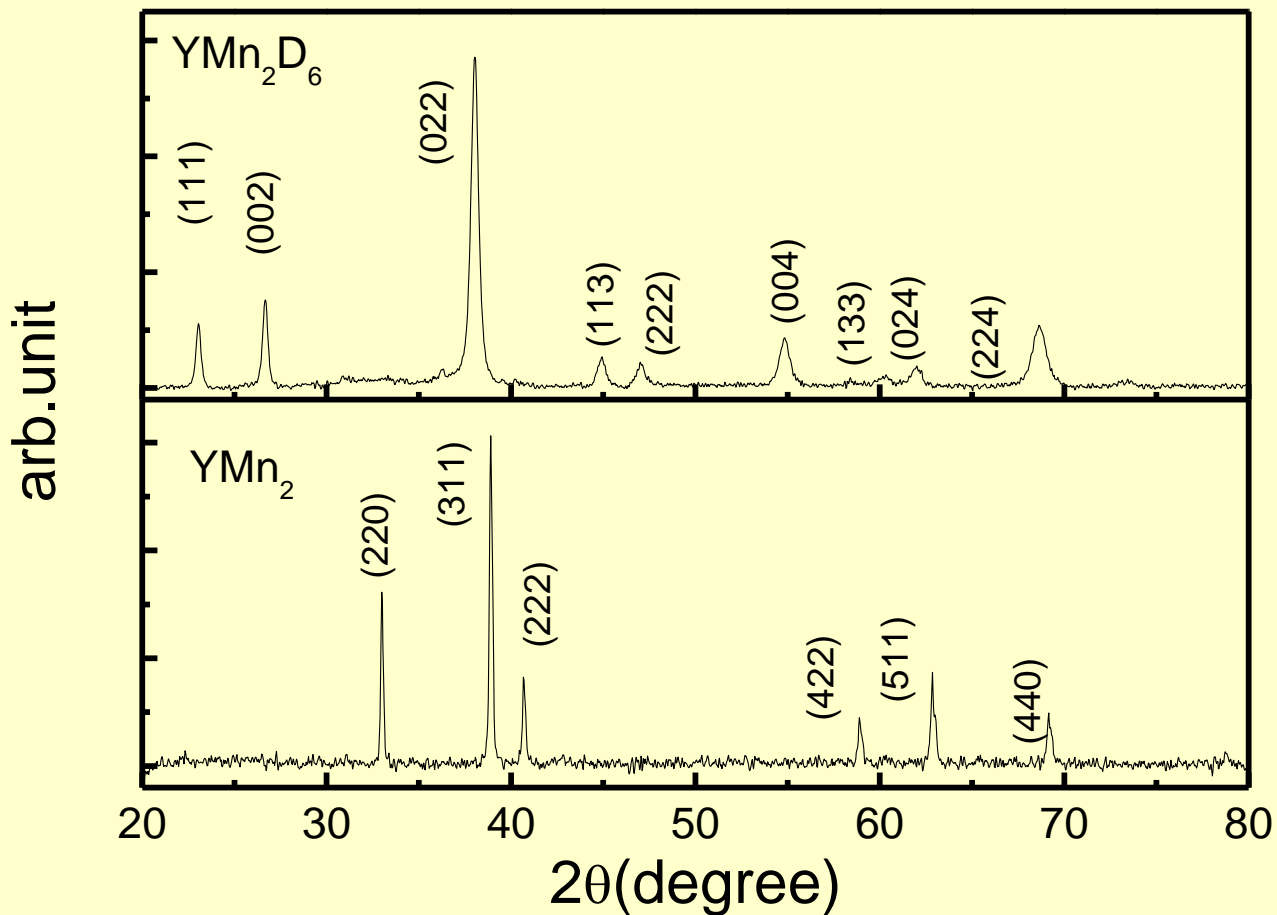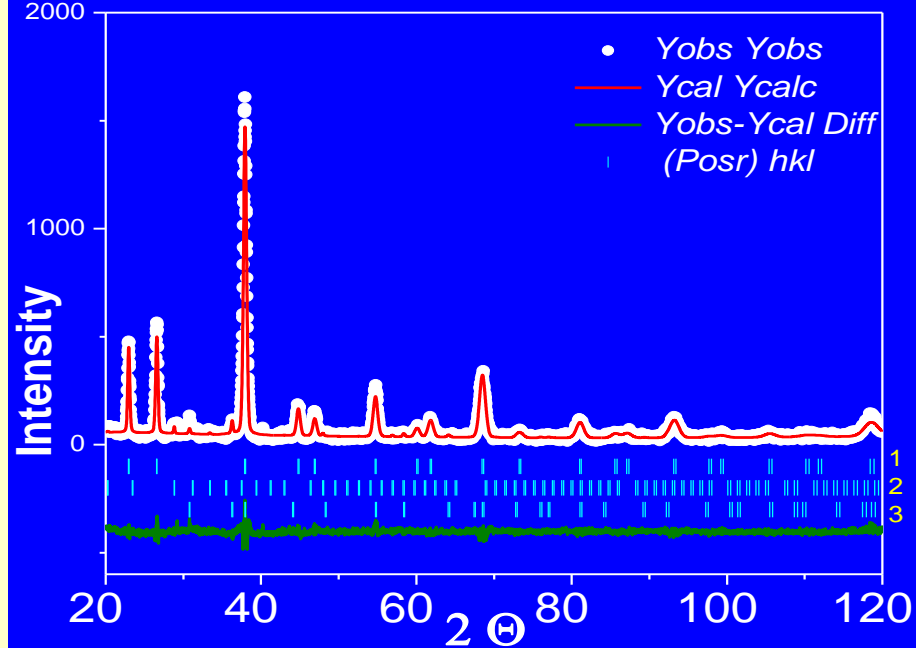
Rietveld refinement for XRD pattern of YMn_2D_6.
Phases: 1) YMn_2D_6, 2) Y_2O_3, 3) $YMn_2D_{4.5}$

Table : XRD results for YMn_2D_6

Sample	Space group	Lattice parameters	
YMn_2	Fd3m	a=7.681 Å	400.06 Å³
YMn_2D_6	Fm3m	a=6.709 Å	299.34 Å³

V. Paul-Boncour, S.M. Filipek, M. Dorogova, F. Bourée, G. André, I. Marchuk, A. Percheron-Guégan, R. S. Liu , J. Sol.State Chem. 178 (2005)

Formation of YMn_2D_6 (cubic *Fm3m)* from YMn_2 (C15) .
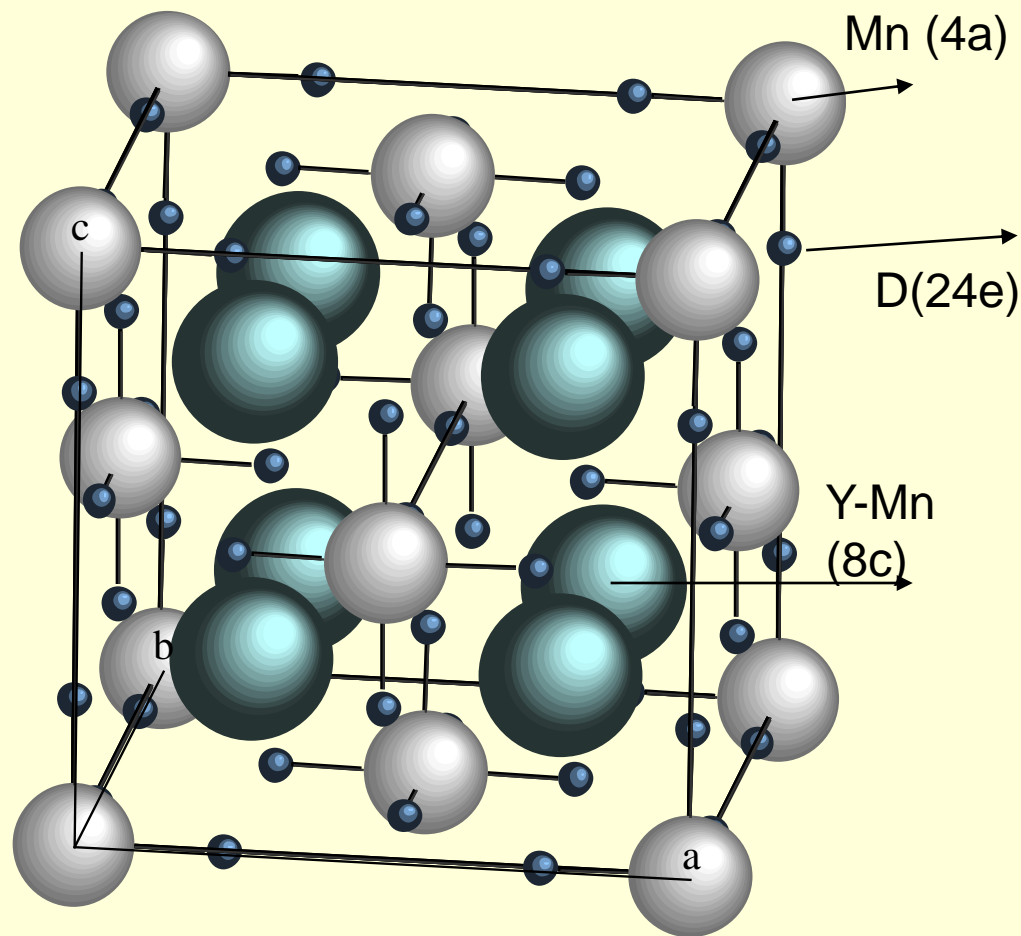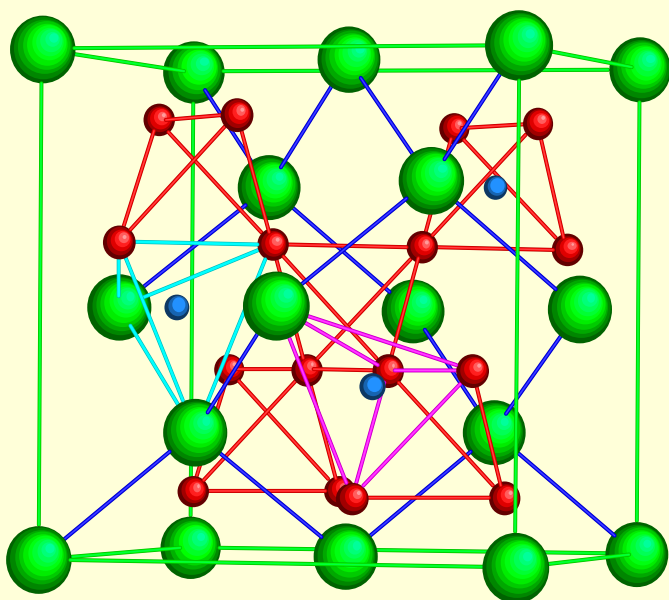
New hydride YMn_2H_6

- A new phase YMn_2D_6 was synthesized by submitting YMn_2 to 1.7 kbar deuterium pressure at 473 K. According to X ray (XRD) and neutron powder diffraction (NPD) experiments, YMn_2D_6 crystallizes in the K_2PtCl_6-type cubic structure with a =6.709(1) Å at 300 K. The Y and half of the Mn atoms occupy statistically the 8c site whereas the other Mn atoms are located in 4a site and surrounded by 6 D atoms (24 e). No ordered magnetic moment is observed in the NPD patterns and the magnetization measurements display a paramagnetic behaviour. The study of the thermal stability by Differential Scanning Calorimetry and XRD experiments indicates that this phase decomposes in YD_2 and Mn at 625 K, and is more stable than $YMn_2H_{4.5}$.

Differential Scanning Calorimetry
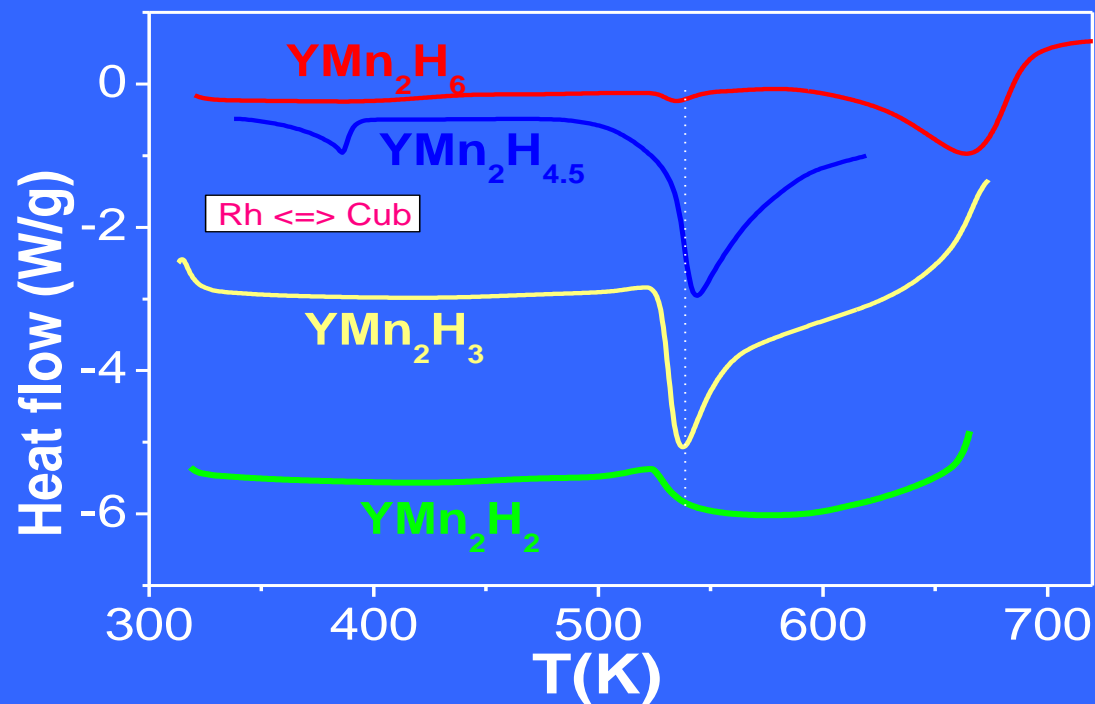
Evolution of the DSC signal versus temperature for YMn$_2$H$_2$, YMn$_2$H$_3$, YMn$_2$H$_{4.5}$ and YMn$_2$D$_6$

The large endothermic peak observed in YMn$_2$D$_6$ (T$_{max}$= 664 K and H=200±2 J/g) can be attributed to the decomposition into YD$_2$ and α-Mn which is complete at 673 K

V. Paul-Boncour, S.M. Filipek, M. Dorogova, F. Bourée, G. André, I. Marchuk, A. Percheron-Guégan, R. S. Liu, , J. Sol.State Chemistry 178 (2005) 356
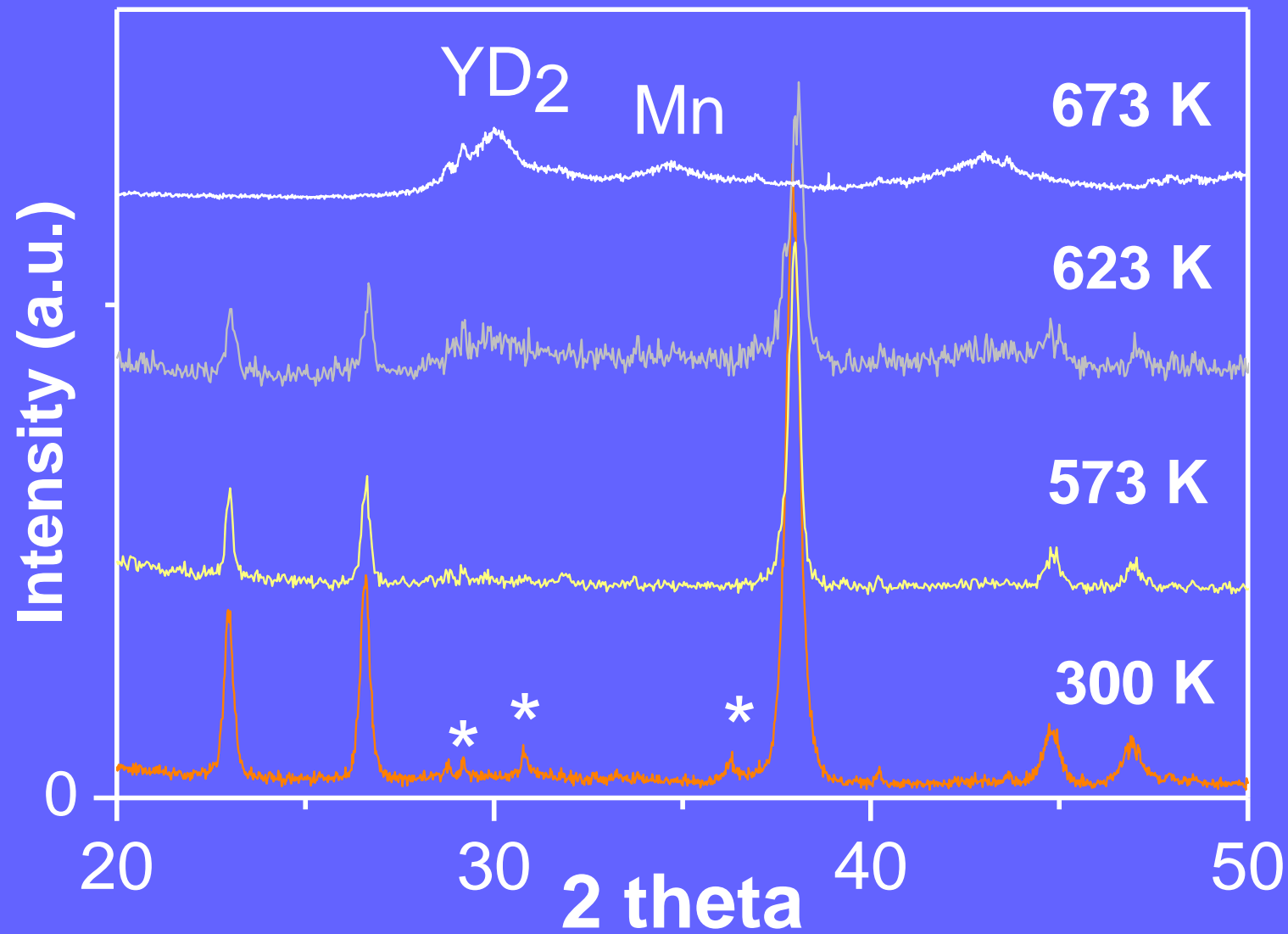
Evolution of the YMn_2D_6 patterns after various DSC treatments. The temperatures correspond to the DSC experiment maximum temperatures.

Table: XRD results for YMn_2D_6 after DSC experiments

Tmax (K)	phase	%	cell parameter	Remarks
298	YMn_2D_6 YMn_2D_x Y_2O_3	91 7 2	a = 6.709 Å a = 8.210 Å	
523	YMn_2D_6 YMn_2D_x Y_2O_3	87 8 5	a = 6.707 Å a = 8.200 Å	
573	YMn_2D_6	100	a = 6.7050 Å	Additional lines have disappeared
593	YMn_2D_6 YD_2	62 38	a = 6.705 Å	
623	YMn_2D_6 YD_2 Mn	22 35 42	a = 6.688 Å	small particles
673	YD_2 Mn	44 55		broad lines due to the small size of the diffracting domain
723	YD_2 Mn	44 55		
873	$Y_2Mn_2O_7$			

V. Paul-Boncour, S.M. Filipek, M. Dorogova, F. Bourée, G. André, I. Marchuk, A. Percheron-Guégan, R. S. Liu, , J. Sol.State Chemistry 178 (2005) 356

New hydride YMn_2H_6

➤ **The random (Y, Mn) substitution on the 8c site is rather surprising due to the difference of the metallic atomic radius between the Y (1.80 Å) and the Mn (1.35 Å) atoms. However this can be related to the fact that this phase has been obtained with a complete reorganization of the atom location under pressure.**

➤ **The deuterium atoms are not located into interstitial sites (A2B2 or AB3) like in other YMn_2H_x hydrides but form octahedra around the Mn2 atoms. The distances between the D atoms (d=2.34 Å) are larger than the Switendick criterium d=2.1 Å, whereas the Mn2-D distances (1.65 Å) are shorter than the sum of the atomic metallic radius (1.75 Å). The Mn1 and Y atoms have 12 D neighbors at 2.37 Å.**

V. Paul-Boncour, S.M. Filipek, M. Dorogova, F. Bourée, G. André, I. Marchuk, A. Percheron-Guégan, R. S. Liu, , J. Sol.State Chemistry 178 (2005) 356

New hydride YMn_2H_6; Mn-H bonding

➤ **The Mn2-D distances (d(Mn-D) = 1.65 Å) are close to those observed in other M_2TH_6 hydrides. For example, in Mg_2FeH_6, d(Fe-D) 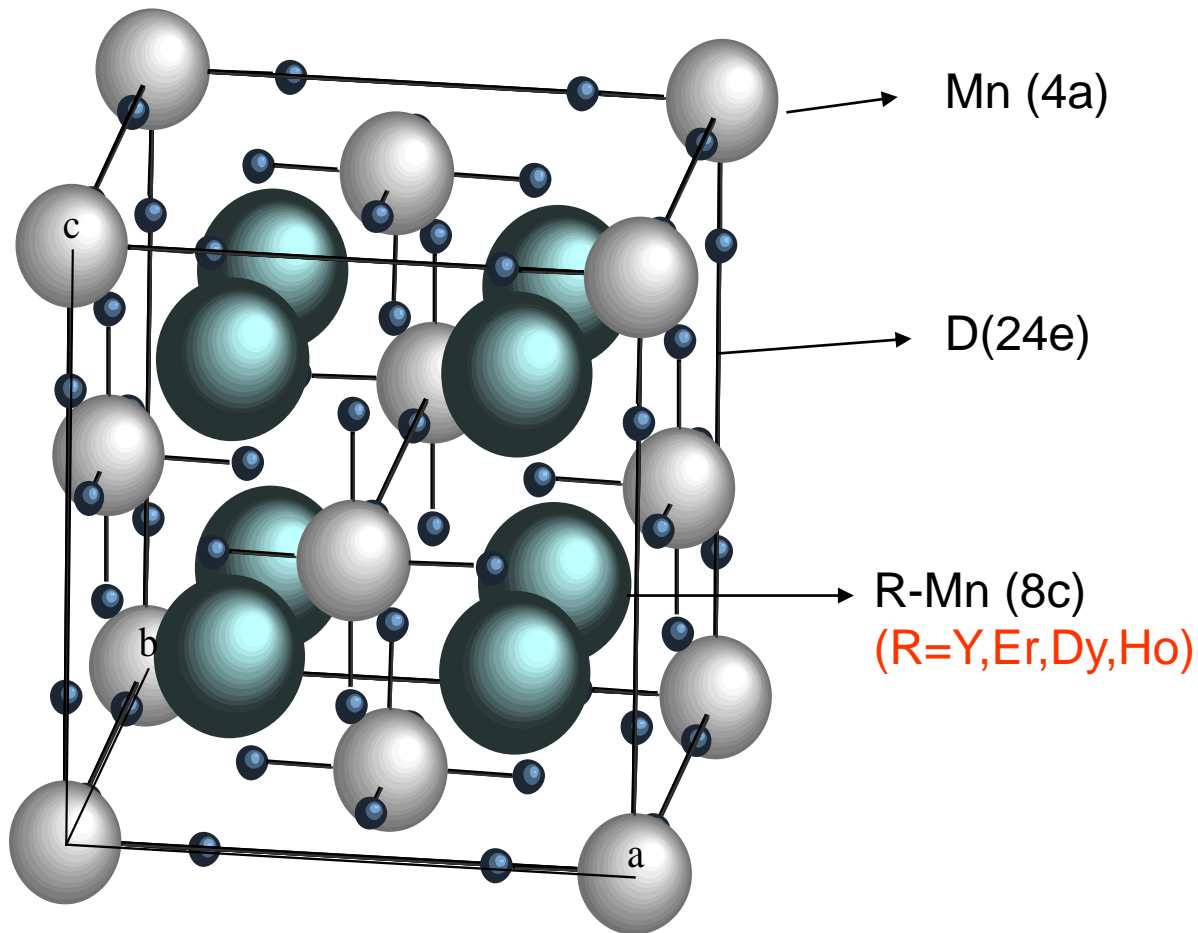= 1.556 Å and in Mg_2OsH_6, d(Os-D) = 1.682 Å. These short distances are indicative of covalent bonding. These hydrides can therefore be considered as coordination compounds rather than interstitial metal hydrides. In addition these M_2TH_6 compounds are described as complex anions TH_6^{4-} surrounded by a cage of divalent M^{2+} cations. Assuming the same type of electronic configuration for YMn_2D_6, one should suppose that the Mn atoms surrounded by the D atoms (Mn2) are Mn^{2+} whereas the Mn on the 8c site (Mn1) should be Mn^+, if we consider that the Y atoms are Y^{3+}.**

V. Paul-Boncour, S.M. Filipek, M. Dorogova, F. Bourée, G. André, I. Marchuk, A. Percheron-Guégan, R. S. Liu, , J. Sol.State Chemistry 178 (2005) 356

Under influence of hydrogen the Laves phases C15+C14 ($DyMn_2$, $HoMn_2$) and C14 ($ErMn_2$) would transform into…?
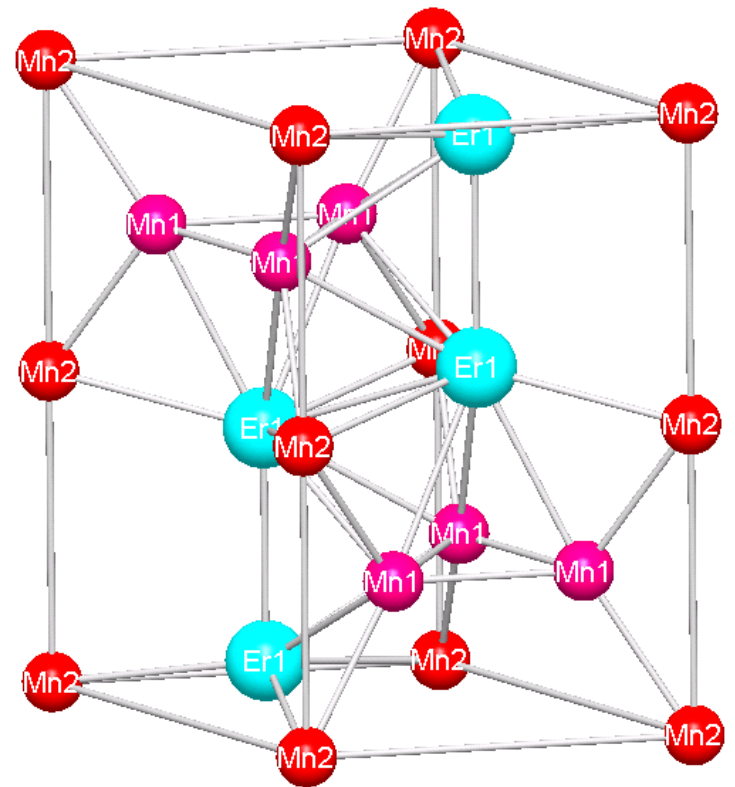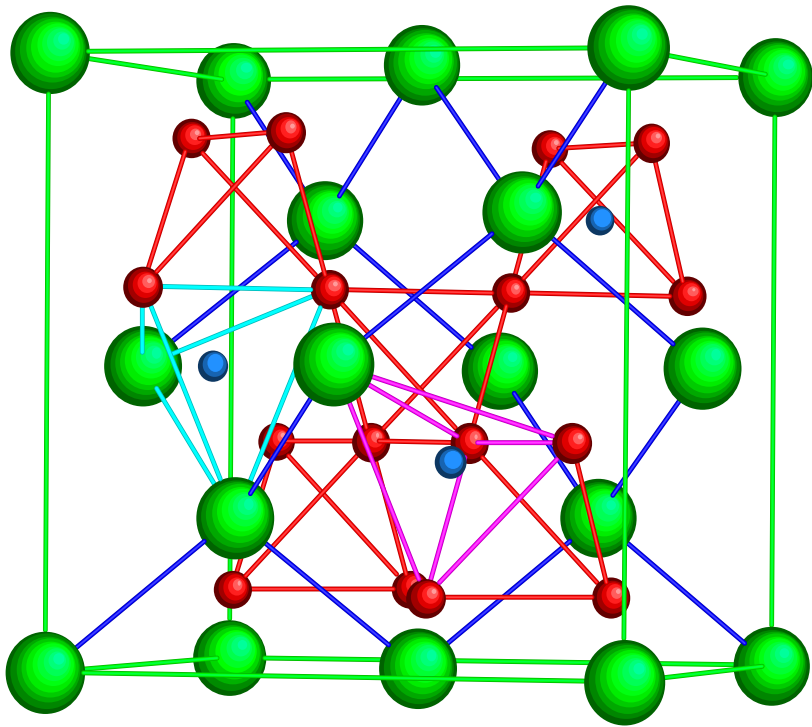
…the same structure as YMn_2D_6 (Fm3m) through complex rearrangement of the (C15 or C14!!) lattice!!!

Mn (4a)

D(24e)

R-Mn (8c)
(R=Y,Er,Dy,Ho)

YMn_2D_6

$ErMn_2D_6$

$DyMn_2D_6$

$HoMn_2D_6$

S.M. Filipek, H. Sugiura, V. Paul-Boncour, R. Wierzbicki, I. Marchuk Studies of Novel Deuterides RMn2D6 (R – Rare Earth) compressed in DAC up to 30 GPa *submitted to J. Phys.C.; Condens. Matter*

Experimental and refined NPD pattern of ErMn₂D₆ at 300K
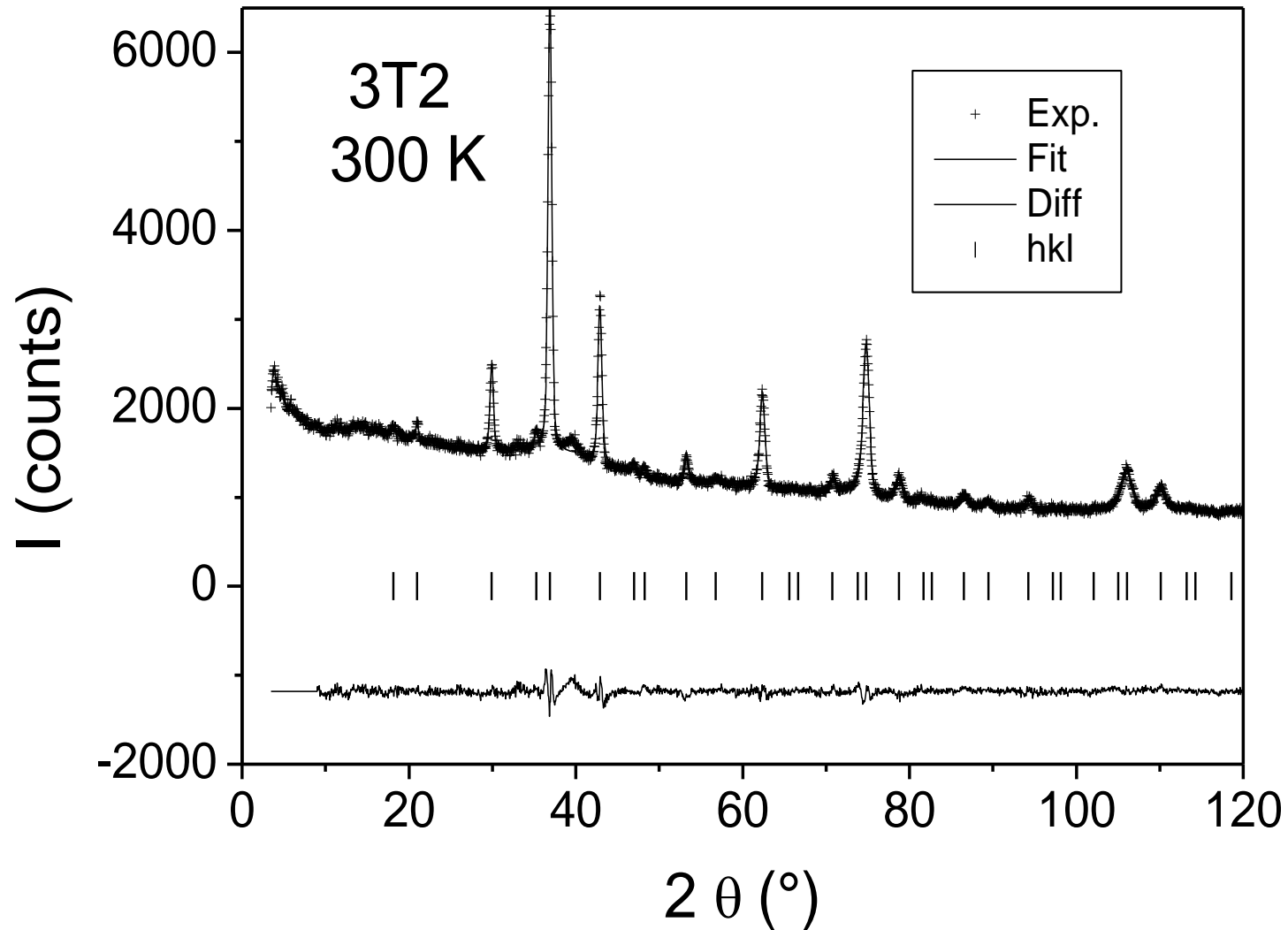
V Paul-Boncour, S M Filipek, G André, F Bourée, M Guillot, R Wierzbicki, I Marchuk, R S Liu, B Villeroy, A Percheron-Guégan, H.D. Yang, S. C. Pin, J.Phys.: Condens. Matter **18** (2006), 6409-6420.

Novel $ErMn_2D_6$ deuteride

➤ A new phase $ErMn_2D_6$ has been prepared by applying high hydrogen pressure on C14 $ErMn_2$. This phase is isostructural to YMn_2D_6 and crystallizes in a disordered fluorite structure with Er and half the Mn atoms randomly substituted on the same 8c site and the other Mn atoms forming octahedral MnD_6 units. This complex hydride is very stable and decomposes into ErD_3 and Mn at about 630 K. The reverse susceptibility follows a Curie Weiss law with an effective moment of 10 µB similar to that of $ErMn_2$. But although a saturation magnetization of 4 µB, which is half that of $ErMn_2$ at 2 K is observed, no long range magnetic order was found in the NPD patterns. However short range order corresponding to both ferromagnetic and antiferromagnetic correlations are observed up to 5 K. The chemical disorder of Er and Mn atoms on the 8c site should prevent the long range order and favours a distribution of Er spins orientation.

V. Paul-Boncour, S.M. Filipek *et al.* J. Phys.: Condens. Matter 18 (2006) 6409–6420

DSC curves of YMn_2D_6 and $ErMn_2D_6$ measured with a speed of 20 K/mn.

V. Paul-Boncour, S.M. Filipek *et al.* J. Phys.: Condens. Matter 18 (2006) 6409–6420
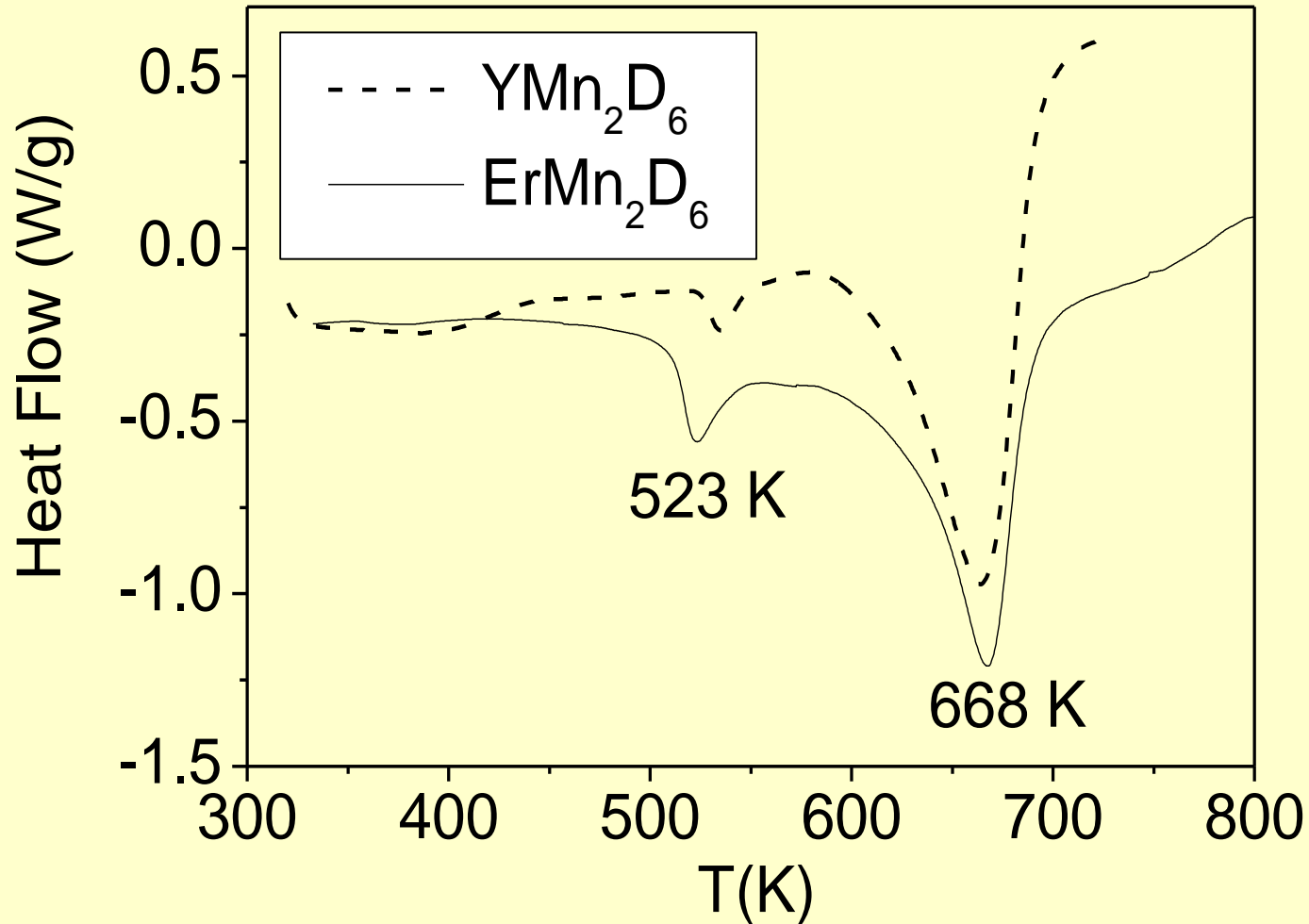
Table. Structural properties of RMn_2 and RMn_2D_6 compounds (R= Er, Y, Ho and Dy)							
Compound	Structure; percentage	A (Å)	c(Å)	V(Å^3)	Z	V/Z (Å^3)	$\Delta V/V_0$(%)[a]
YMn$_2$	C15; 100%	7.6791		452.82	8	56.60	
YMn$_2$D$_6$	Fm-3m, 100%	6.7083		301.89	4	75.47	33.33[c]
DyMn$_2$	C14; 4%	5,3606	8,7343	217,36	4	54,34	
	C15; 95%	7.5872		436,76	8	54,59	
DyMn$_2$D$_6$	Fm-3m; 100%	6.720		303.52	4	75.88	39,63[b] 38.98[c]
HoMn$_2$	C14; 19%	5,3269	8,6885	213,51	4	53,38	
	C15; 80 %	7,5430		429,17	8	53,65	
HoMn$_2$D$_6$	Fm-3m; 100%	6.677		297.78	4	74.44	39,46[b] 38.77[c]
ErMn$_2$	C14, 100%	5.2949	8.6446	209.90	4	52.47	
ErMn$_2$D$_6$	Fm-3m, 100%	6.6796		298.04	4	74.51	42.00[b]

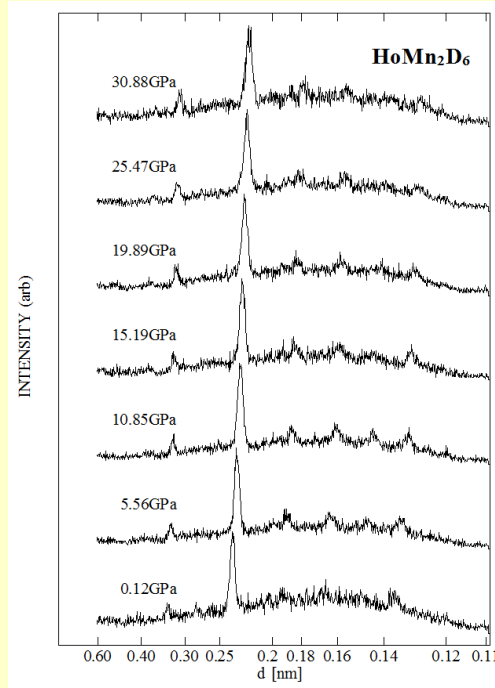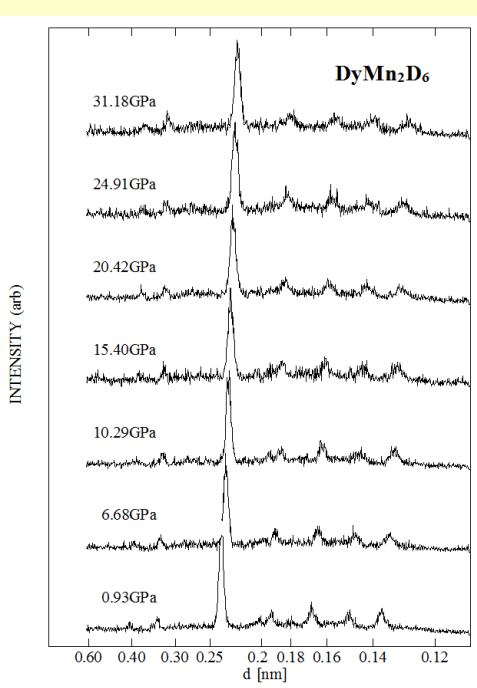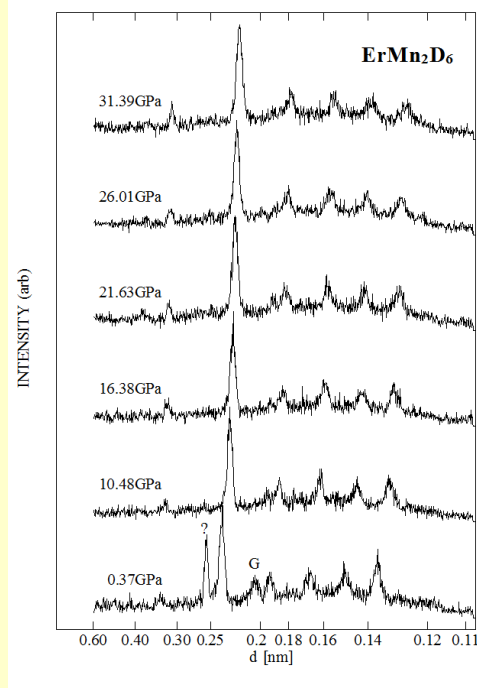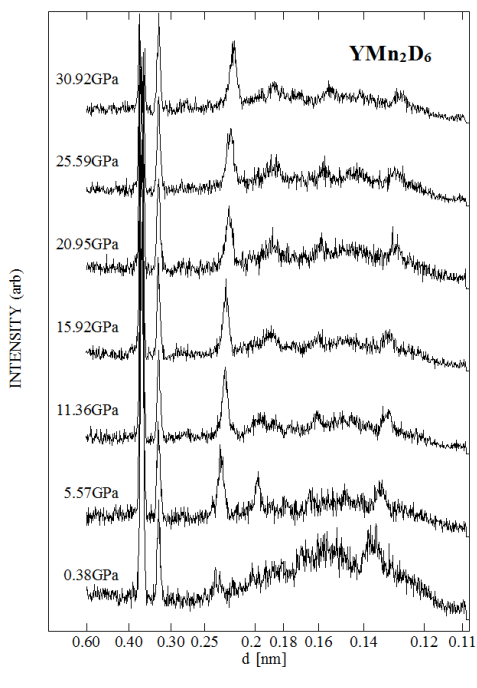[a]Variation of the molecular volume: $\Delta V/V_0 = (V_{deuteride} - V_{parent})/V_{parent}$
[b]Value calculated with respect to the parent C14 structure.
[c]Value calculated with respect to the parent C15 structure.

The YMn$_2$D$_{1.15}$ and YMn$_2$D$_2$ undergoes spinodal like phase separation; at the highest pressure limit (30 GPa) the amount of hydrogen enriched phase is estimated at 34% for YMn$_2$D$_{1.15}$ and 59% for YMn$_2$D$_2$, respectively. YMn$_2$D$_x$ (where x=3.4 or 4.0) do not decompose but high value of $K0$ at initial pressure range is still observed just like in its parent (hydrogen free YMn2) compound. The bending near 8 GPa observed in the compression curves reflects that the bulk modulus of these compounds should change

For the right figure:
YMn$_2$H$_6$
V_0 [cm^3/mol] = 45.35
K_0 [GPa] = 68.05
K_0' = 6.28

Left figure labels:
1: YMn$_2$D$_4$
2: YMn$_2$D$_4$
3: YMn$_2$D$_{3.4}$
4: YMn$_2$D$_{3.4}$
5: YMn$_2$D$_2$
6: YMn$_2$D$_1$
7: YMn$_2$
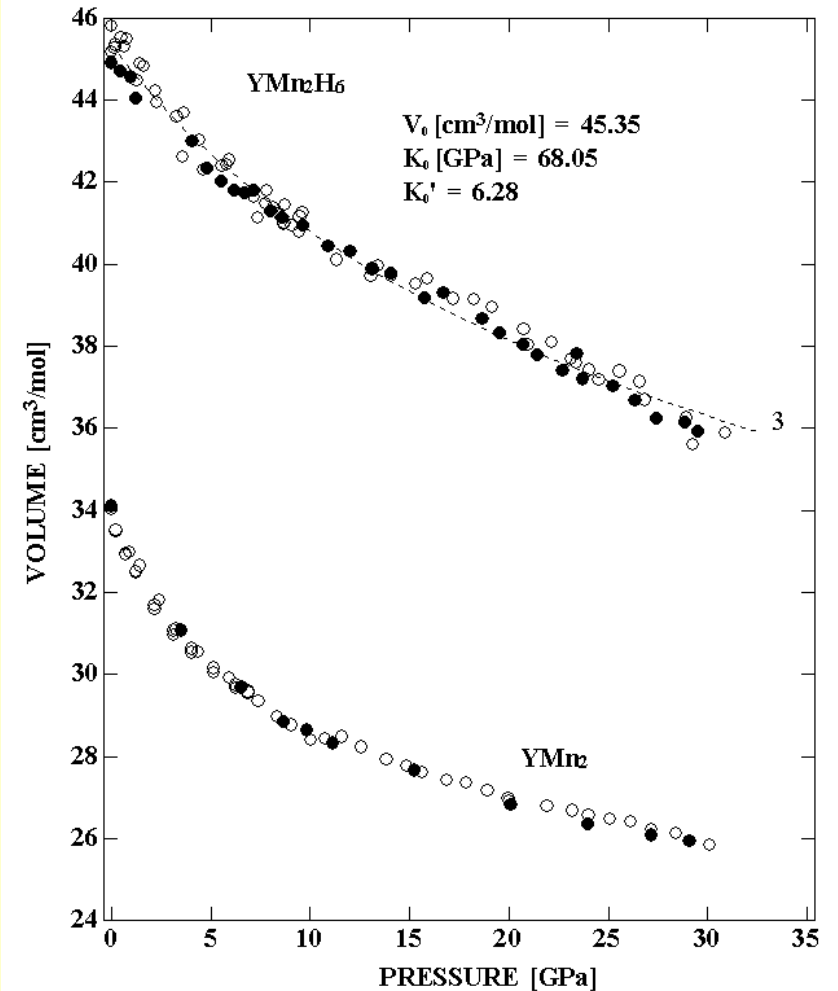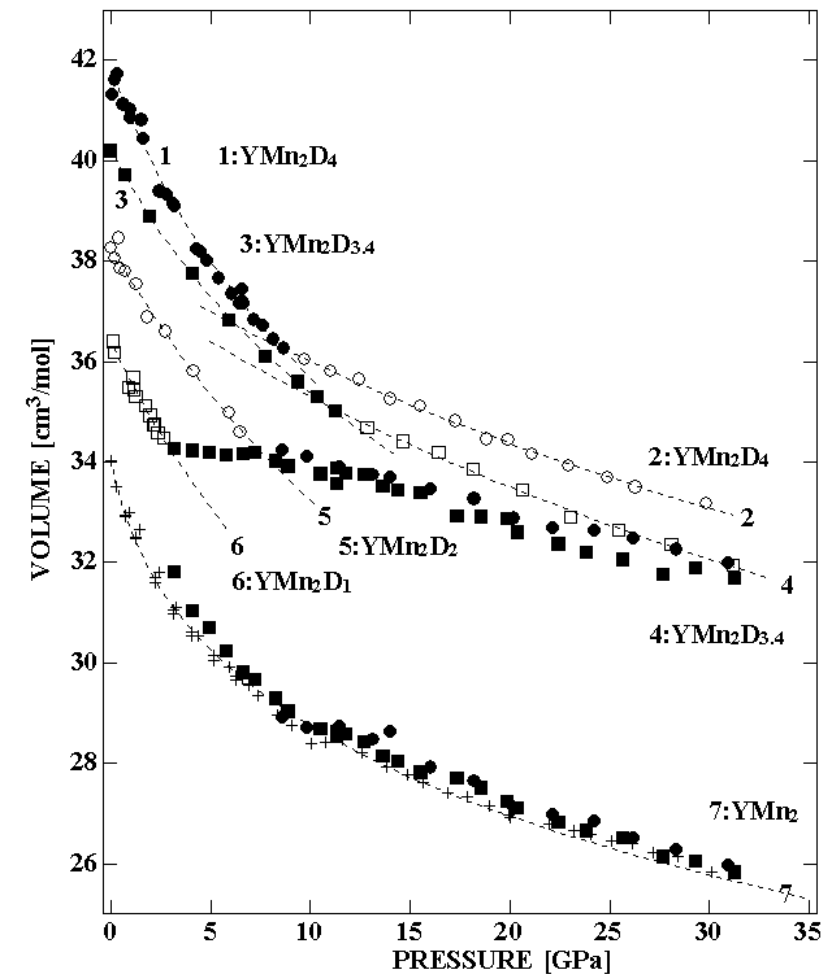
Energy dispersive patterns of YMn$_2$D$_6$; ErMn$_2$D$_6$; DyMn$_2$D$_6$ and HoMn$_2$D$_6$ taken at different pressures
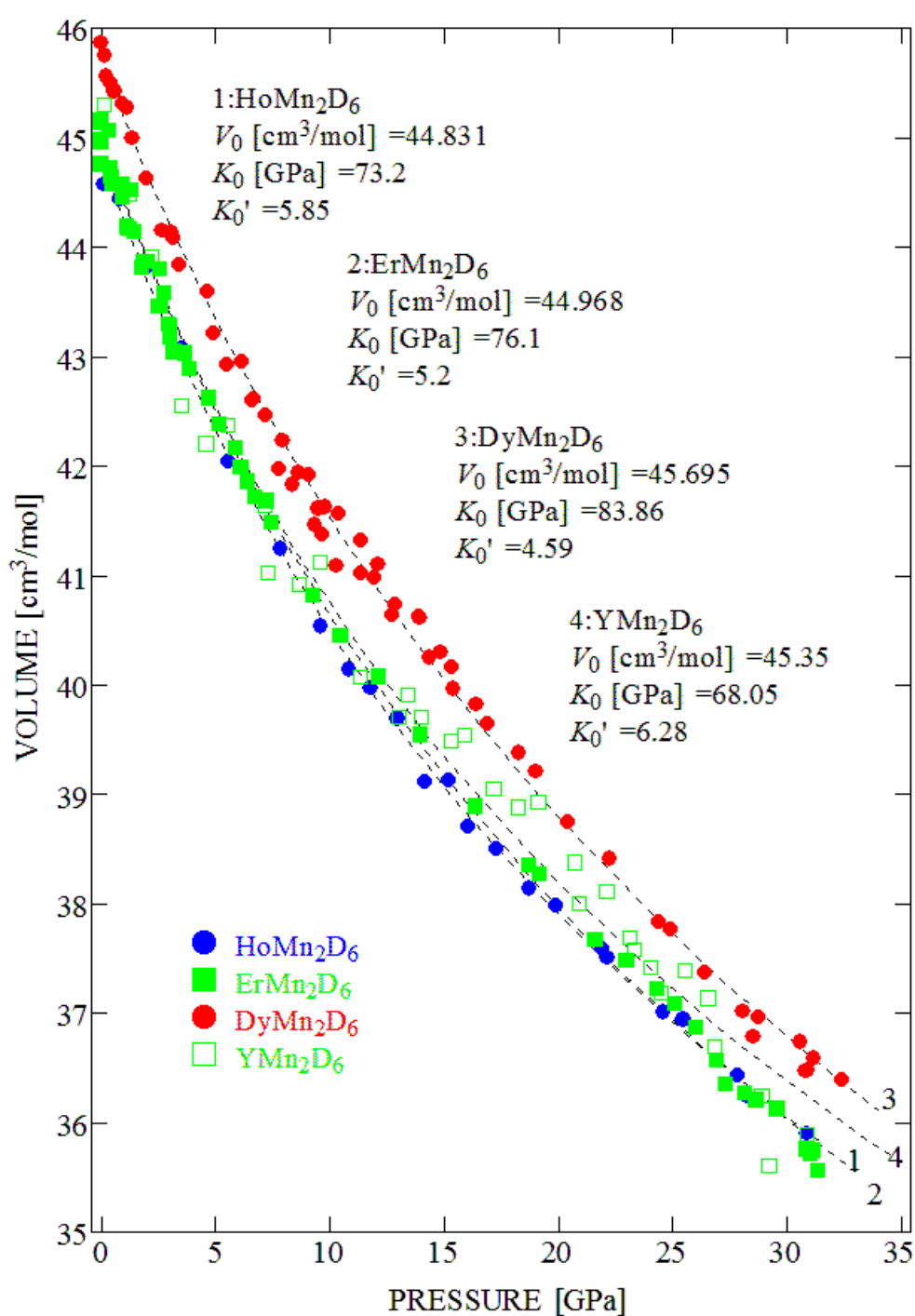
Pressure dependence of the molar volume of $HoMn_2D_6$, $ErMn_2D_6$, $DyMn_2D_6$ and YMn_2D_6.

Figure labels and data:

1:$HoMn_2D_6$
$V_0 [cm^3/mol] = 44.831$
$K_0 [GPa] = 73.2$
$K_0' = 5.85$

2:$ErMn_2D_6$
$V_0 [cm^3/mol] = 44.968$
$K_0 [GPa] = 76.1$
$K_0' = 5.2$

3:$DyMn_2D_6$
$V_0 [cm^3/mol] = 45.695$
$K_0 [GPa] = 83.86$
$K_0' = 4.59$

4:YMn_2D_6
$V_0 [cm^3/mol] = 45.35$
$K_0 [GPa] = 68.05$
$K_0' = 6.28$

Legend:
● $HoMn_2D_6$
■ $ErMn_2D_6$
● $DyMn_2D_6$
□ YMn_2D_6

Axis labels: VOLUME [cm³/mol] (vertical), PRESSURE [GPa] (horizontal)

EOS parameters of RMn_2 and RMn_2D_x deuterides (R = Y, Dy, Ho and Er) K_0 and K_0' are bulk modulus and its first derivative

Sample	Vo cm3/mol	Ko [GPa]	Ko'	n	Remarks	Refer.
YMn₂	34.02	21.6	13.2	21	*Cubic* C15 (low pressure segment *P*<8GPa)	[1]
	31.24	83.1	7.13	29	*Cubic* C15 (high pressure segment *P*>8Gpa)	
YMn₂D₃,₄	40.11	60.28	4.0 fixed	11	*Cubic C15* (low pressure segment *P*<8GPa)	
	37.80	133.9	4.0 fixed	20	*Cubic* C15 (high pressure segment *P*>8Gpa)	
YMn₂D₄	41.65	46.07	4.0 fixed	27	*Rhombohedral* (low pressure segment)	
	38.22	153.0	4.0 fixed	17	*Rhombohedral*(high pressure segment)	
YMn₂D₆	45.35	68.05	6.28		*cubic* Fm-3m (whole range)	
DyMn₂	33,01	63.2	6.1		Cubic (C15)	[2]
DyMn₂D₆	45.69	83.8	4.59	60	*cubic* Fm-3m (whole range)	
HoMn₂	32,31				*C15 + C14*	
HoMn₂D₆	44.83	73.2	5.85	23	*cubic* Fm-3m (whole range)	
ErMn₂	31,6				*C14*	
ErMn₂D₄.₆	40.65	79.2 (2)	4 fixed		*hexagonal*	[3]
ErMn₂D₆	44.97	76.1	5,20	50	*cubic* Fm-3m (whole range)	
n –number of points						

[1].Sugiura H, Paul-Boncour V, Percheron-Guégan A, Marchuk I, Hirata T, Filipek S M, Dorogova M 2004 *J. Alloys Compd*, **367** 230.
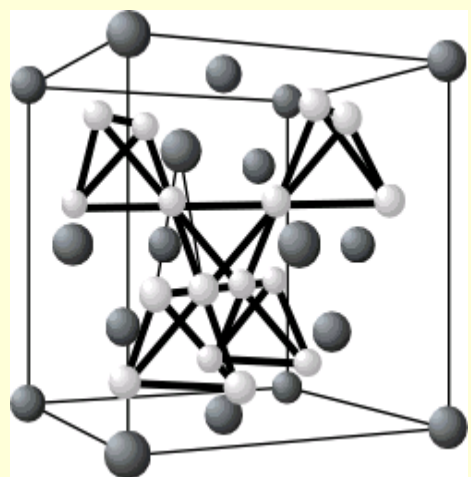[2] Reiss G, Dissertation, February 2000 University of Paderborn
[3] Makarova O L, Goncharenko I N and Le Bihan T 2004 *Sol. State Comm.* **132** 329,
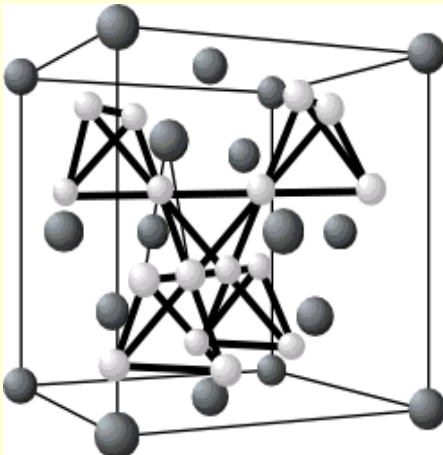
Novel Hydrides in Laves phases

S.M. Filipek et al. J.Phys, Cond.Matter, 14 (44) 11261 (2002)

Cubic (C15, $F\bar{d}3m$)
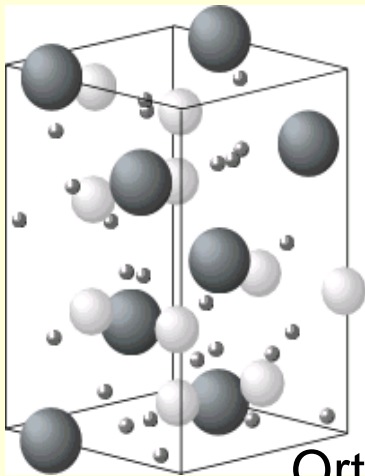
ZrFe$_2$
ZrCo$_2$
ErFe$_2$
YFe$_2$
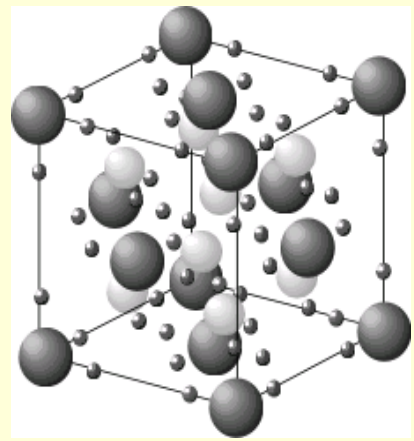YMn$_2$

Hydrogenation under high pressure hydrogen

Cubic ($F\bar{d}3m$)
ZrFe$_2$H$_4$
ZrCo$_2$H$_2$

Orthorhombic ($Pmn21$)
ErFe$_2$D$_5$
YFe$_2$D$_5$

Cubic ($F\bar{d}3m$)

YMn$_2$D$_6$

Summary and Conclusions

- Treatment of RMn_2 Laves phases by using high hydrogen pressure resulted in discovery of novel hydrides including group of isostructural hydrides RMn_2D_6 formed in a process of dramatic rearrangement of the parent metallic lattice.

- RMn_2D_6 hydrides have complex structure of Fm-3m symmetry with $(Mn^ID_6)^{5-}$ anions and disordered location of R and Mn1 atoms in 8c positions independently of the parent structure. Such hydrides have never been obtained from Laves compounds.

- RMn_2D_6 phases have unusually high stability due to bonding character different from interstitial hydrides. Compression curves of this new family of hydrides goes smoothly excluding possiblity of phase transitions. All EOS curves are located close each other but differ from those received for hydrides with smaller H (D) content. Bulk moduli of all RMn_2D_6 do not differ much and have values comparable with those of the parent compounds.

- Further work: Search for new hydrides/deuterides (RMn2D6 and other) also in pseudobinary systems.

Short comment about recent discovery of room temperature superconductivity in LuHnNy

Drozdov, A. P., Eremets, M. I., Troyan, I. A., Ksenofontov, V. & Shylin, S. I. Conventional superconductivity at 203 kelvin at high pressures in the sulfur hydride system. Nature 525, 73 (2015)

M. Kostrzewa, K. M. Szczęśniak, A. P. Durajski, R. Szczęśniak, From LaH10 to room–temperature superconductors, Scientific Reports (2020) 10:1592

F. Peng *et al.,* Hydrogen Clathrate Structures in Rare Earth Hydrides at High Pressures: Possible Route to Room-Temperature Superconductivity, Phys. Rev. Lett. (2017) 119, 107001

A. Majumdar *et al.* Superconductivity in FeH5, Phys. Rev. B 96, 201107(R) (2017) and Phys. Rev. Materials **4,** 084005

T. Palasyuk, M. Tkacz, Pressure-induced structural phase transition in rare-earth trihydrides. Part I. (GdH 3, HoH 3, LuH 3), *Solid State Communications* (2005) 133(7):481-486
High-pressure X-ray diffraction studies of gadolinum, holmium and lutetium trihydrides have been carried out in a diamond anvil cell up to 30GPa at room temperature. A reversible structural phase transformation from the hexagonal to cubic phase has been observed for all the hydrides investigated.

Short comment about recent discovery of room temperature superconductivity in LuHnNy

N. Dasenbrock-Gamon *et al.,* Evidence of near-ambient supercoductivity in a N-doped lutetium hydride, Nature (2023)

More than a hundred samples (metallic Lu or LuH2); samples were loaded into the DAC with the H2/N2 gas mixture (99:1) and pressed to 2 GPa. The sample was heated overnight at 65 C. After 24 hours the DAC was released to recover the sample.

Success rate of measuring a sample with superconducting properties was about 35 %.

The exact amount, location and nature of the nitrogen is not specified.

It was not explained what was the difference between the samples (there were 35%) in which the occurrence of superconductivity was found and the remaining samples.

Recently, a number of papers have been published in which the authors negatively verified the report on superconductivity in lutetium hydride.

The precious contribution of all Friends and Colleagues, especially from:
- Institute of Physical Chemistry PAS
- Institute of High Pressure Physics PAS
- Tokyo Institute of Technology
- Institut de Chimie et des Matériaux CNRS Thiais (Paris)
- National Taiwan University (Taipei)
- Ben-Gurion University (Beer Sheva)

is very much appreciated

Thank you very much for your kind attention